# "Vector Chromatography": Modeling Micropatterned Separation Devices

by

Kevin David Dorfman

B.S., The Pennsylvania State University (1999)

Submitted to the Department of Chemical Engineering
in partial fulfillment of the requirements for the degree of

Master of Science

at the

MASSACHUSETTS INSTITUTE OF TECHNOLOGY

June 2001



Signature of Author . . . . . .
Department of Chemical Engineering
15 May 2001

Certified by . . . . . .
Howard Brenner
Willard H. Dow Professor of Chemical Engineering
Thesis Supervisor

Accepted by . . . . . .
Robert Cohen
St. Laurent Professor of Chemical Engineering
Chairman, Committee for Graduate Students

# "Vector Chromatography": Modeling Micropatterned Separation Devices

by

Kevin David Dorfman

Submitted to the Department of Chemical Engineering
on 15 May 2001, in partial fulfillment of the
requirements for the degree of
Master of Science

## Abstract

A repetitive sequence of quiescent fluid layers of differing viscosities through which small spherical Brownian particles move is analyzed so as to illustrate in a simple context how the theory of macrotransport processes, a generalization of Taylor dispersion theory, may be employed to rigorously analyze spatially periodic micropatterned chromatographic separation devices for circumstances in which the solute species to be separated are animated by the action of species-specific external forces oriented asymmetrically relative to the body-fixed pattern. In the generic "vector" separation scheme, illustrated by our elementary example, the different species undergoing separation move, on average, in different directions relative to pattern-fixed axes, whence their chromatographic sorting is effected according to their different mean angular trajectories through the device. This scheme differs fundamentally from traditional "scalar" chromatographic separation schemes, wherein all species move on average parallel to the animating force (including circumstances in which they are passively entrained in a unidirectional solvent flow) and hence for which the sorting is effected by the relative speeds of the several species through the chromatographic column.

Vector chromatography is quantified by two global "macrotransport coefficients," namely the solute mobility dyadic $\overline{\mathbf{M}}^*$ (representing the tensor proportionality coefficient between the mean solute velocity vector $\overline{\mathbf{U}}^*$ and the external force vector $\mathbf{F}$ acting upon the solute molecules) and the dispersivity dyadic $\overline{\mathbf{D}}^*$ (resulting from the deviation of the instantaneous position of the particle from its mean position based upon its mean velocity vector). In the present example these coefficients are studied parametrically as functions of: (i) the orientation of the external force relative to the symmetry axis of the fluid layers; (ii) the local viscosity distribution within a layer; (iii) the *vector* particle Peclet number (constructed from the vector force, the length of the viscosity period, and the Boltzmann factor $kT$); and (iv) the thermodynamic interphase solute partition distribution coefficient between the two fluid layers comprising a unit cell.

Thesis Supervisor: Howard Brenner
Title: Willard H. Dow Professor of Chemical Engineering

# Acknowledgements

I would like to thank Professor Brenner for his useful insights in the preparation of this work, in particular his insistance on "democracy" and emphasis on the fundamentals. In addition, the support of the entire Brenner group was greatly appreciated.

This work was partially supported by a Graduate Research Fellowship from the National Science Foundation to KDD and a grant to HB from the Office of Basic Energy Sciences of the US Department of Energy, as well as a "Grand Challenge Award" from the Mathematical, Information and Computational Sciences Division within the Office of Computational and Technology Research of the Office of Energy Research of the DOE.

# Contents


**1 Introduction** **6**

**2 Physical Description** **12**

**3 Microscale Formulation** **17**

**4 Macroscale Formulation** **21**

4.1 Chromatographic Mobility . . . . . 25

4.2 Dispersivity . . . . . 29

4.3 Macroscale Solution . . . . . 30

**5 Chromatographic Mobility** **32**

5.1 Continuous Periodic Viscosity Case . . . . . 32

5.1.1 Calculation of $P_0^\infty$ . . . . . 32

5.1.2 Calculation of $\overline{\mathbf{M}}^*$ . . . . . 33

5.1.3 Sinusoidal Viscosity Function . . . . . 34

5.2 Immiscible Layered Case . . . . . 37

5.2.1 Calculation of $P_0^\infty$ . . . . . 38

5.2.2 Calculation of $\overline{M}_\perp^*$ . . . . . 40

5.2.3 Calculation of $\overline{M}_\parallel^*$ . . . . . 42

5.2.4 Angular Separation . . . . . 44

**6 Dispersivity** **52**

6.1 Continuous Periodic Viscosity Case . . . . . 52

6.1.1 Calculation of $B_\perp$ . . . . . 53
6.1.2 Calculation of $B_\parallel$ . . . . . 54
6.1.3 Calculation of $\overline{\mathbf{D}}^*$ . . . . . 56
6.2 Immiscible Layered-Fluid Case . . . . . 58
6.2.1 Calculation of $B_\perp$ . . . . . 59
6.2.2 Calculation of $B_\parallel$ . . . . . 60
6.2.3 Calculation of $\overline{\mathbf{D}}^*$ . . . . . 61
6.3 Immiscible Layered-Fluid Case (Dominant Brownian Motion) . . . . . 64
6.3.1 Calculation of $\overline{D}^*_{\perp\perp,m}$ . . . . . 66
6.3.2 Calculation of $\overline{D}^*_{\parallel\parallel,m}$ . . . . . 67

**7 Concluding Remarks** **68**

# Chapter 1

# Introduction

The present contribution is the first of a projected series dealing with the modeling of vector chromatographic separation schemes in micropatterned devices. Such devices, in particular "obstacle course" microlithographic arrays [1-5], have received considerable attention in recent years in connection with their use as chromatographic separation media. These arrays are constructed by etching a spatially periodic sequence of raised obstacles onto a polymer mask, using microlithography techniques pioneered in the production of microelectronic devices. Since the microlithographic process produces a repeated pattern on the substrate, it is convenient to refer generically to such devices as being a subset of the larger class of micropatterned devices. By the phrase "micropatterned" is meant that there exists at the "pore-level" or "interstitial-scale" a space-fixed spatially periodic (microscale) structure, be it an array of obstacles [1-5], entropic traps [6], a microscale polymer gel matrix [7, 8], or the repetitive viscosity field studied in this paper.

The solute is assumed animated within the (otherwise quiescent) solvent-filled pores of the micropatterned device by an external force field acting solely on the solute particles, typically a steady or pulsed electric field acting on charged solute molecules. Attention is confined in the present paper to steady force fields, where species-specific hydrodynamic and/or physiochemical interactions of the different solute species with the micropatterned obstacles provide the chromatographic separation mechanism. The dilute solution, single Brownian particle theory to be discussed assumes that solute-solute interactions, be they colloidal or hydrodynamic, are negligible compared with solute-solvent and solute-obstacle interactions (i.e. "wall" effects).

Previously referred to as "rectified Brownian motion" [9], the generic separation processes embodied within this general technique should, in our opinion, be more appropriately termed "vector chromatography." The chromatographic aspect of the separation process is obvious, since solute molecules are separated by size or some other distinguishing physiochemical feature, such as charge or adsorptive affinity towards the surfaces of the fixed obstacles. The vectorial aspect of the separation refers to the crucial importance of the mean *direction* of net solute motion (relative to axes fixed in the micropatterned chips) traversed by a given class of particles or species under the action of the externally applied force field, when the direction of the force is oriented at an angle relative to the periodic micropattern. This contrasts with conventional "scalar" or "unidirectional" chromatographic schemes (affinity chromatography, hydrodynamic chromatography, etc.), in which the separation derives from the different mean *speeds* of the several species through the separation medium, all of which move on average in the same direction. In the class of devices addressed here, the separation is effected through the different mean *angles* adopted by the different species moving relative to the fixed axes of the micropatterned device (and, perhaps, the different solute speeds too, if some fortuitous combination of properties were to give rise to the same trajectory angle). As such, we are distinguishing between "vector" and "scalar" chromatography in the sense that, now, the *direction* of the mean solute velocity vector $\overline{\mathbf{U}}_j^*$, say, of a given species $j$ acquires importance beyond its mere *magnitude*, $\left|\overline{\mathbf{U}}_j^*\right|$ — the latter being the relevant parameter in conventional scalar, or unidirectional, chromatography, where the different speeds of the several solute species constitute the sole mechanism for effecting the separation. As a result, the phrase "directional chromatography" constitutes an alternate appellation for the separation scheme under discussion here.

One of the more promising features of vector chromatography lies in the possibility for its use in effecting *continuous* (vs batch) separation. Austin and coworkers [1, 3, 5] successfully constructed an obstacle course for DNA electrophoresis which demonstrated that the species are separated spatially due to their different mean angular trajectories through the course, as well as temporally due to their different mean speeds. Since DNA or other molecules of different end-to-end lengths exit the device at different locations on the periphery of the micropatterned "chip," the process can be run continuously. This contrasts with batch processing — a time-

consuming, labor-intensive and, concomitantly, expensive scheme.

Disorder inevitably exists in the internal arrangement of "obstacles" within conventional (i.e. non-periodically arrayed) chromatographic columns in present use owing to their more-or-less random packing. In particular, widely-used gel electrophoretic columns result in geometrically irreproducible local (microscale) obstacle configurations. In contrast, microlithographic arrays possess highly regular, controllable, periodically-ordered, pore-scale features. Accordingly, the configurational randomness that limits the efficacy of gel electrophoresis and other conventional chromatographic separation schemes is eliminated in micropatterned devices, assuring sharper, more cleanly-defined separations. Such devices offer the possibility of optimal designs for specified separation tasks by controlling the geometrical arrangement of the obstacles, perhaps even their physiochemical surface features too, such as their adsorptivity with respect to specified solutes.

Presently, the design of such vector, micropatterned separation chips lacks a rational basis, with much of the pertinent literature reporting only construction techniques and observed experimental separation efficiencies for a given pattern, solute-solvent system, and set of operating conditions [3, 7, 10]. Several theoretical explanations of the separation characteristics of micropatterned devices have been proposed [9, 11], but they are fundamentally irrational owing to their *ad hoc* incorporation of diffusion effects, as well as in the inappropriate implicit assumption of position-independent and isotropic mobilities at the interstitial- (i.e. microscale-) phenomenological level of description of the pertinent solute transport phenomena. Moreover, these schemes are intrinsically unable to predict the extent of dispersion accompanying the separation process. More explicitly, although rough estimates of mean particle trajectories are possible based on essentially macroscale arguments, in the absence of a rational scheme for formulating and subsequently "homogenizing" the underlying microscale transport equations to determine dispersion and accompanying band broadening (which are macroscale characteristics), it is impossible to estimate the degree of sharpness of the chromatographic separation scheme.

To remedy these theoretical shortcomings, generalized Taylor dispersion (macrotransport) theory [12] may be employed to analyze and interpret the vector chromatographic separation of Brownian solute particles moving under the influence of externally applied force fields through

the interstices of micropatterned, spatially periodic devices filled with an otherwise quiescent viscous solvent. This theory constitutes a rigorous physico-mathematical scheme for calculating, *inter alia*, the averaged, long-time, asymptotic behavior of finite-sized Brownian particles moving through solvent-saturated periodic media. The phrase "long-time" is meant to imply that a Brownian particle has had ample time to sample all accessible *local* positions within a representative unit cell before exiting the system ("chip"). In the context of microlithographic arrays, this postulates that a solute tracer has sampled all accessible points within a composite unit cell many times, although not the points within *every* cell of the array. Explicit criteria for quantifying the phrase "long-time" are available [12]. Thus, with $l$ a characteristic dimension of the unit cell, $\|\mathbf{D}\|$ a norm of the molecular diffusivity of the Brownian particle through the homogeneous solvent, and $t$ the time required to sample the points within a unit cell, the criterion requires that $t \gg l^2/\|\mathbf{D}\|$. Since a typical obstacle course on a chip constitutes thousands of unit cells [3], this long-time assumption will almost certainly always be met in practice, since, all other things being equal, the greater the number of cells, the longer the time spent by the particle within the system boundaries.

With but a single exception [13], the present work is distinguished from previous macrotransport analyses [12] primarily in that solute movement relative to the fixed obstacles is animated solely by an external force acting directly upon the solute molecules themselves, rather than by their passive, piggy-back convective entrainment within a solvent flowing through the interstices between the obstacles. The ensuing mean stochastic motion of a particular solute species will be seen to be characterized by a body-fixed, species-specific macroscale chromatographic mobility dyadic $\overline{\mathbf{M}}^*$, serving as the tensorial phenomenological proportionality coefficient between the coarse-grained mean solute velocity vector $\overline{\mathbf{U}}^*$ of that species and the external force vector $\mathbf{F}$ exerted upon the Brownian solute molecules comprising that species:

$$\overline{\mathbf{U}}^* = \overline{\mathbf{M}}^* \cdot \mathbf{F}. \tag{1.1}$$

In the subsequent analysis, the external force acting on a solute particle will be expressed in

component form,

$$\mathbf{F} = \mathbf{i}_x F_x + \mathbf{i}_y F_y + \mathbf{i}_z F_z, \tag{1.2}$$

with Cartesian unit vectors $(\mathbf{i}_x, \mathbf{i}_y, \mathbf{i}_z)$ in the $(x, y, z)$ directions, respectively, and with position- (and time-) independent components $(F_x, F_y, F_z)$. Subsequent papers in the series will examine the case of time-periodic forces [12].

As this contribution constitutes the first in a contemplated series outlining how vector chromatographic separations in micropatterned devices can be rationally analyzed from first principles, we have chosen to illustrate the generic macrotransport scheme by means of a computationally tractable example — one whose relatively simple closed-form solution structure unequivocally demonstrates the utility of generalized Taylor dispersion theory as a tool in such analyses. The requisite calculations for more geometrically realistic (and hence less analytically tractable) systems cannot generally be effected in closed form, but will, rather, inevitably require extensive, parameter-specific numerical computations, whose exhaustive detail cannot help but obscure the basic simplicity of the overall generic macrotransport scheme itself. Future papers in this series will deal numerically with these more realistic micropatterns, presenting results whose often counter-intuitive conclusions and implications will necessarily lack the relative transparency of the present illustrative example. It is for this reason that we have chosen the layered viscous fluid example which follows, despite the fact that such a spatially periodic configuration is physically unrealizable in practice owing to the fluid-mechanical instability of such an arrangement.

In spite of the fact that the model problem subsequently discussed may not be physically realizable, it nevertheless encapsulates the essential physics underlying the concept of vector chromatography. Explicitly, the process features spatially periodic, locally inhomogeneous microstructure in the form of a repetitive viscosity (mobility) variation. Moreover, the model problem possesses an anisotropic mobility on the local scale since the layered fluids comprising the unit cell are bounded in the $z$-direction, but unbounded in the $x$- and $y$-directions. The similarity between this variable viscosity scheme and other micropatterned separation schemes analyzed elsewhere [9,11] is readily apparent, inasmuch as the etched silicon micropat-

terns described in the latter references are spatially periodic and result in position-dependent, anisotropic local mobilities owing to the hydrodynamic effect of the solid obstacles on the motion of the solutes being separated. Moreover, the analysis presented herein is readily applicable to any micropatterned device featuring external force fields and local anisotropy [1-8], as the fundamental physical principles involved are identical.

We proceed by initially outlining the exactly-posed physical problem to be analyzed, beginning with a microscale description of the pertinent transport phenomena involved — namely a detailed, unsteady-state, convective-diffusive, initial- and boundary-value problem posed locally at the interstitial scale, $l$, say. The overwhelming intractability of this unsteady, initial value *microscale* problem, even for the relatively simple geometric configuration posed by our layered-fluid system, motivates the subsequent generalized Taylor dispersion analysis, which permits extracting the $L$-scale ($L \gg l$) *global* or macroscale features of the overall chromatographic solute transport process on the length scale $L$ of the chip, *without the necessity for first having to solve the underlying $l$-scale (microscale) problem posed.* In this latter context, we begin by presenting generic formulae whereby the macroscale velocity vector $\overline{\mathbf{U}}^*$ (or, equivalently, the mobility dyadic $\overline{\mathbf{M}}^*$) and dispersivity dyadic $\overline{\mathbf{D}}^*$ for a given species may be calculated from the prescribed microscale data, formulated for the motion of a Brownian tracer in an external force field $\mathbf{F}$ in the absence of bulk (i.e. macroscale) solvent motion. The remainder of the paper is then devoted to explicitly calculating these macroscale phenomenological coefficients for our layered-fluid example, and establishing the functional dependence of these coefficients upon the prescribed microscale parameters and geometry. Following this, we discuss the fundamental role of these tensorial macrotransport coefficients in interpreting micropatterned vector chromatography. As an aside, we also comment on the general inapplicability of a macroscale Nernst–Plank-Einstein-type relationship, $\overline{\mathbf{D}}^* = kT\overline{\mathbf{M}}^*$, relating the macroscale dispersivity and mobility (except in the weak-force, essentially purely hindered molecular diffusion case, where they are indeed related by such an expression). This lack of correlation between these two key phenomenological parameters reflects the fact that, with the exception of the circumstances cited in the previous sentence, one's ability to extract the dispersive characteristics of the solute particle's trajectory from the essentially hydrodynamic knowledge embedded in the mobility $\overline{\mathbf{M}}^*$ is lost.

# Chapter 2

# Physical Description

As in Figure 2-1a, consider the creeping motion of a single spherical Brownian particle of radius $a$ moving under the influence of an external vector force $\mathbf{F}$ through an otherwise quiescent fluid characterized by a spatially periodic viscosity field $\mu$. The fluid, which is regarded as being unbounded, may be envisioned as a series of unit cells, repeating in all three spatial dimensions. The most convenient choice of a unit cell, shown in Figure 2-1b, is a repeating rectangular parallelepiped of length $l_z$ in the $z$-direction and (arbitrary) $x$- and $y$-lengths, $l_x$ and $l_y$, respectively, in the transverse direction, such that the superficial volume $\tau_0$ of a unit cell is

$$\tau_0 = l_x l_y l_z. \tag{2.1}$$

As the unit cell is an arbitrary, albeit convenient, mathematical construct rather than a material physical entity, the results ultimately obtained for the physically-objective entities $\overline{\mathbf{M}}^*$ and $\overline{\mathbf{D}}^*$ must necessarily prove to be independent of the particular choice made for the repetitive unit cell shape, as is indeed known to be a generic consequence of macrotransport theory [12].

The viscosity, regarded as being functionally dependent only upon $z$, and otherwise uniform in the $x$-$y$ plane, is thereby taken to be of the general form $\mu(x, y, z) = \mu(z)$.[1] This viscosity

[1]It is implicitly assumed that the translational motion of the particle through the fluid does not sensibly disburb this viscosity distribution. This approximation is obviously globally valid for the case where the sphere radius $a$ is small compared with the period $l_z$. It is especially reasonable in circumstances where the periodic viscosity distribution stems from the existence of alternating layers of immiscible fluids, stacked one atop the

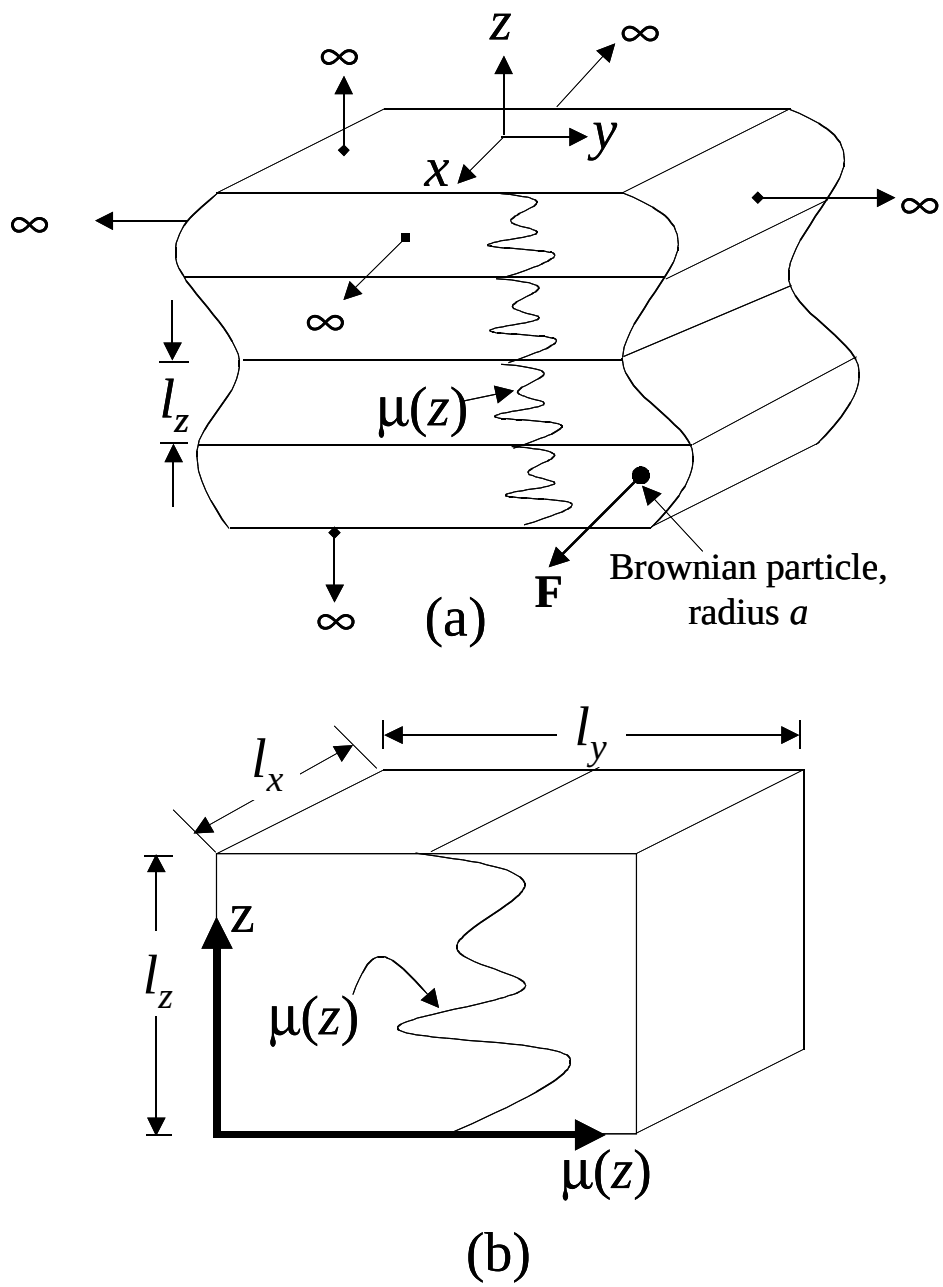


Figure 2-1: (a) Infinitely-extended inhomogeneous fluid possessing a continuous spatially periodic variable viscosity $\mu = \mu(z)$ of period $l_z$; (b) a unit cell of the medium: ($0 < x < l_x$, $0 < y < l_y$, $0 < z < l_z$ ). Also shown is a spherical Brownian particle of radius $a$ ($a \ll l_z$ ).

field repeats itself periodically with a period $l_z$, such that

$$\mu(z) = \mu(z + l_z) \quad (-\infty < z < \infty). \tag{2.2}$$

As a special case of the above, involving alternating layers of two immiscible fluids, each separately of uniform viscosity (Fig. 2-2), the intracell viscosity field is given piecewise by the expression

$$\mu(z) = \begin{cases} \mu_1 = \text{const.} & (0 < z < \epsilon_1 l_z), \\ \mu_2 = \text{const.} & (\epsilon_1 l_z < z < l_z), \end{cases} \tag{2.3}$$

within each cellular domain $0 < z < l_z$. Here, $\epsilon_i = l_i/l_z$ $(i = 1, 2)$, in which $l_i$ is the thickness of the layer of fluid whose viscosity is $\mu_i$, so that $\epsilon_i$ is the fraction of the total (unit cell) volume occupied by fluid $i$. This immiscible layered-fluid model obeys the periodic intercell (i.e. $-\infty < z < \infty$) restriction (2.2). In such circumstances, we assume that the discontinuity (2.3) in viscosity is a manifestation of the presence of two immiscible fluids, and that the Brownian solute molecules do not necessarily form thermodynamically ideal solutions within either solvent phase.[2] Accordingly, on the assumption that local thermodynamic equilibrium prevails at the interface between the two immiscible fluids, a thermodynamic partition coefficient $K$ then relates the solute concentrations (or, equivalently, the subsequent single-particle conditional probability densities) in the respective phases lying immediately on either side of the interface [cf. eq. (3.14)]. In the limit where the solute forms a thermodynamically ideal solution with *both* fluids, one has that $K = 1$.

While we discuss systems that extend indefinitely in all directions, real systems are nec-

other, as in Fig. 2-2. Contact-line singularities [14] may give rise to fundamental questions regarding the detailed mechanism via which the sphere crosses the interface separating these immiscible fluids. In particular, interface deformation on the continuum scale may impact upon the translation of the particle across the boundary between the layers. Properly accounting for the exact behavior at the interface requires adopting a diffuse interface model [15], which implies the introduction of a third length scale. However, the disparities between these length scales (interfacial scale, $l$-scale, and $L$-scale) makes the consideration of effects of translation across the interface irrelevant in the present context, especially since our goal is merely to illustrate the overall macrotransport scheme in a simple context, rather than to unequivocally resolve a pertinent physical problem.

[2]Because of this assumption, and the concomitant issue of solute partitioning between the phases that arises, the limiting case where $\mu_1 = \mu_2 = \text{const.} = \mu$, will prove not to be physically identical to the case of a single homogeneous fluid of viscosity $\mu$ unless the interphase partition coefficient $K$ [cf. eqs. (3.14)-(3.15)] has the value unity.

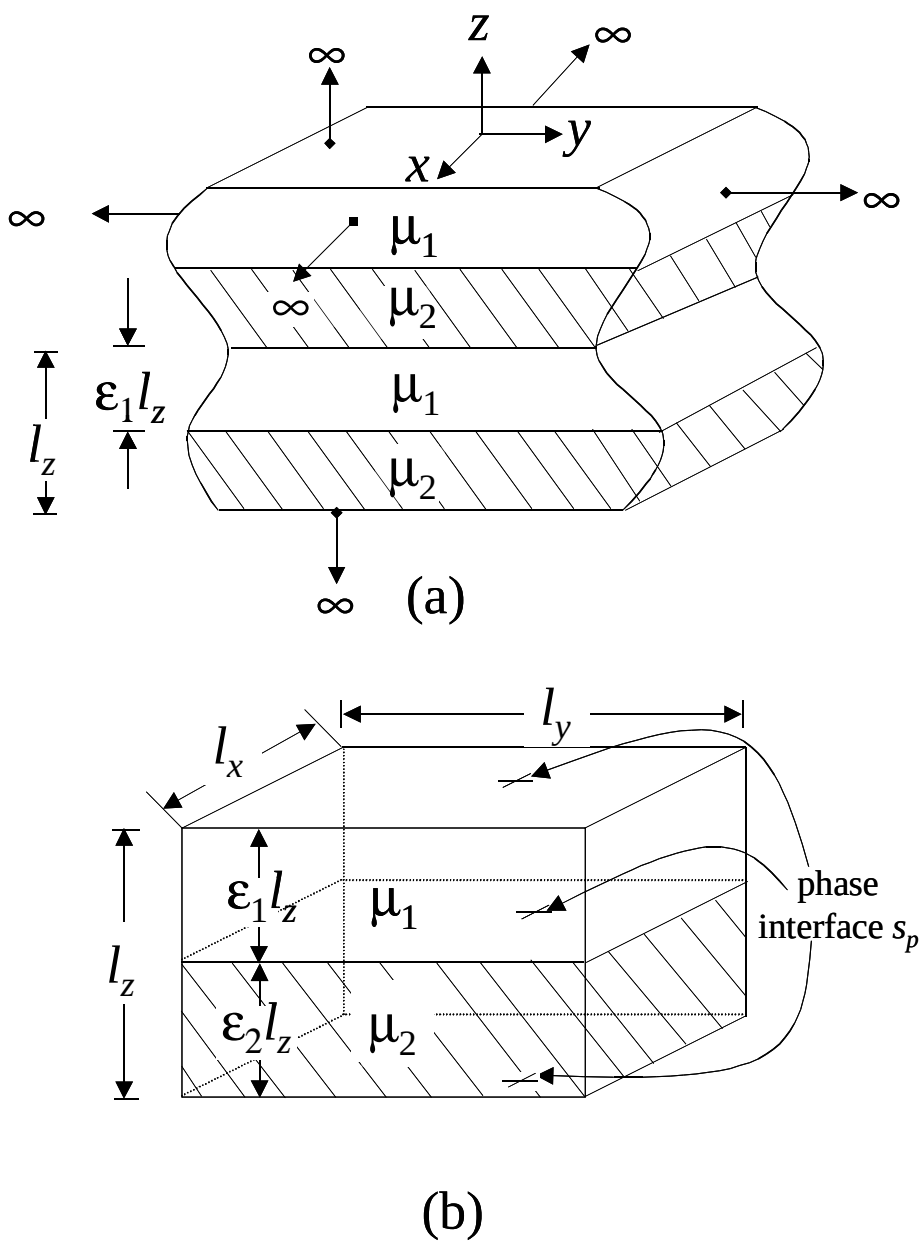


Figure 2-2: (a) Infinitely-extended two-layered fluid with spatially periodic (but locally position-independent) viscosities $\mu_1$ $(0 < z < \epsilon_1 l_z)$ and $\mu_2$ $(\epsilon_1 l_z < z < l_z)$; (b) a unit cell of the medium.

essarily of finite extent, with $L$, say, representing a characteristic linear global dimension of the bounded system (e.g. the length or width of the micropatterned chip). Our results are expected to apply in all circumstances for which the inequality

$$\frac{l_z}{L} \ll 1 \tag{2.4}$$

prevails.

In circumstances wherein $a/l_z \ll 1$, the local microscale Stokes-law translational velocity vector $\mathbf{U}(x, y, z)$ of a spherical particle of radius $a$ moving under the action of the net external force $\mathbf{F}$ (including buoyant forces, if any) imposed upon it is

$$\mathbf{U} = \mathbf{M} \cdot \mathbf{F} \ . \tag{2.5}$$

With the sphere (center) situated at position $z$, and with the inequality $a\,\mathrm{d}(\ln \mu)/\mathrm{dz} \ll 1$ assummed to apply (except possibly at the interface between immiscible fluids), the microscale mobility and diffusivity tensors are given by the respective Stokes law and Stokes-Einstein expressions,

$$\mathbf{M} = \mathbf{I}M(z), \quad M^{-1} = 6\pi\mu(z)a, \tag{2.6a}$$

$$\mathbf{D} = \mathbf{I}D(z), \quad \mathbf{D} = kT\mathbf{M}, \tag{2.6b}$$

with $\mathbf{I}$ the unit isotropic tensor, $k$ Boltzmann's constant, and $T$ the absolute temperature.[3]

[3]We use the tensorial forms of the microscale mobility $\mathbf{M}$ and diffusivity $\mathbf{D}$ despite their isotropic and, hence, scalar nature in present circumstances (i.e. in the assumed absence of "boundary" or "wall" effects resulting from the presence of the interfaces in the layered case) to later emphasize the fact that the effective or macroscale solute mobility $\overline{\mathbf{M}}^*$ [cf. (5.7)] and macroscale dispersivity $\overline{\mathbf{D}}^*$ [cf. (6.17)] dyadics of the solute through the composite system are each anisotropic. (Were microscale wall effects properly incorporated into our equations, the microscale mobility and diffusivity would be anisotropic too.)

# Chapter 3

# Microscale Formulation

This section outlines the detailed microscale formulation underlying the transport of a single spherical Brownian solute tracer particle moving through the interstices of a micropatterned device filled with an otherwise quiescent viscous solvent of nonuniform viscosity $\mu(z)$. The conditional probability density $P(x, y, z; t|x_0, y_0, z_0) \equiv P(\mathbf{R}; t \,|\, \mathbf{R}_0)$ for finding the center of the Brownian tracer at a specific point $\mathbf{R} \equiv (x, y, z)$ in the infinite domain

$$\mathbf{R}_\infty \equiv (-\infty < x < \infty, -\infty < y < \infty, -\infty < z < \infty) \tag{3.7}$$

at time $t$, given the initial position

$$\mathbf{R}_0 \equiv (x_0, y_0, z_0) \qquad (\mathbf{R}_0 \in \mathbf{R}_\infty) \tag{3.8}$$

of the tracer at time $t = 0$, is given by the solution $P \equiv P(\mathbf{R}; t \,|\, \mathbf{R}_0)$ of the convection-diffusion equation [16]

$$\frac{\partial P}{\partial t} + \nabla \cdot \mathbf{J} = 0, \tag{3.9}$$

with $\mathbf{J}$ the flux density,

$$\mathbf{J} = \mathbf{U}P - \mathbf{D} \cdot \nabla P, \tag{3.10}$$

and satisfying an initial unit pulse input condition,

$$P = \delta(\mathbf{R} - \mathbf{R}_0) \equiv \delta(x - x_0)\delta(y - y_0)\delta(z - z_0) \text{ at } t = 0, \tag{3.11}$$

with $\delta$ the Dirac delta function, and vanishing at spatial infinity:

$$P \to 0 \quad \text{as} \quad |\mathbf{R} - \mathbf{R}_0| \equiv (|x - x_0|, |y - y_0|, |z - z_0|) \to (\infty, \infty, \infty) \quad \forall t. \tag{3.12}$$

Explicitly, one is to solve the equation

$$\frac{\partial P}{\partial t} + \nabla \cdot (\mathbf{U}P) = \nabla \cdot (\mathbf{D} \cdot P) \tag{3.13}$$

together with the initial condition (3.11) in the infinitely-extended fluid domain (3.7), subject to the pertinent flux or concentration boundary conditions imposed at internal system boundaries, if any [cf. eqs. (3.14)-(3.16)], together with the requirement (3.12).[1]

Further internal boundary conditions are required at each interface for the layered-fluid, multiphase case, where the system through which the solute tracer particle moves is composed of pairs of periodically alternating immiscible fluid layers (and with which solvents, "1" and "2", the solute possibly forms non-ideal solutions). Explicitly, at each of the pairs of interfaces identified by the spatial positions $(x, y, z_n = z + nl_z)$ $(n = 0, \pm 1, \pm 2, \dots)$, and with $P_i$ $(i = 1, 2)$ the respective Brownian solute conditional probability density within the fluid of viscosity $\mu_i$, it is required that

$$K_1 P_1(x, y, z_n; t) = K_2 P_2(x, y, z_n; t) \;\; (n = 0, \pm 1, \pm 2, \dots), \tag{3.14}$$

with the interphase partition coefficient $K$ defined as

$$K \stackrel{\text{def.}}{=} \frac{K_1}{K_2}. \tag{3.15}$$

[1]Physically, $P(\mathbf{R}; t \,|\, \mathbf{R}_0)$, which is the Green's function [17] for the differential equation (3.13), is formally equivalent to the local, volumetric solute concentration $c(\mathbf{R}; t)$ that would arise from the impulsive introduction of a concentrated unit mass of solute at the point $\mathbf{R}_0$ at time $t = 0$ into a fluid otherwise initially devoid of solute.

Also required is the continuity of the normal solute flux component across the phase boundary:

$$\upsilon \cdot [\mathbf{J}_1(x, y, z_n; t) - \mathbf{J}_2(x, y, z_n; t)] = 0 \quad (n = 0, \pm 1, \pm 2, \dots), \tag{3.16}$$

with $\upsilon \equiv \mathbf{i}_z$ a unit vector normal to the interface. [In the arguments of $P_i$ and $\mathbf{J}_i$ appearing in (3.14) and (3.16) we have, for notational simplicity, suppressed the argument $(x_0, y_0, z_0)$ appearing in the initial condition (3.11) (which initial points need not lie within the interior of unit cell $n$).]

The innumerable interfacial boundary conditions imposed by eqs. (3.14) and (3.16) for each of the infinitely many $n$'s, and for all time, renders intractable a closed-form solution of the unsteady, initial- and boundary-value microscale problem posed above, at least for the layered case. Moreover, purely numerical approaches towards solving this detailed microscale problem would furnish parameter-specific solutions only for prescribed choices of the parameters, e.g. $\mu_1$, $\mu_2$, $a$, $l_z$, $K$, etc., thereby rendering a comprehensive, wide-ranging parametric study of the ensuing solute separation phenomenon costly. Even more so, these numerical solutions would depend upon the initial local position (3.8) at which the tracer was introduced into a particular one of the infinitely many fluid "layers," a seemingly irrelevant microscale parameter in the course of rationalizing the gross, macroscale behavior of the system. Furthermore, such a scheme would be extraordinarily wasteful of computational resources, since much of the detailed microscale information embodied within the pointwise numerical solution $P(\mathbf{R}; t \,|\, \mathbf{R}_0)$ thereby obtained, in particular its detailed time- and local position-dependence, would clearly be lost in eventually determining the two time- and position-independent physically useful macroscale quantities, $\overline{\mathbf{U}}^*$ (or $\overline{\mathbf{M}}^*$) and $\overline{\mathbf{D}}^*$ via eqs. (4.4)-(4.8), required to quantify the separation process when viewed on a length scale $L$ that is large compared with the length scale $l$ of a cell [cf. eq. (4.1)]. Accordingly, given the overwhelming difficulties faced when attempting to solve the exhaustively-detailed unsteady microscale problem posed above, a purely macroscale, time-independent formulation aimed at calculating $\overline{\mathbf{U}}^*$ and $\overline{\mathbf{D}}^*$ without first having to solve the underlying microscale problem is a choice overwhelmingly to be preferred, provided, of course, that these two parameters can be rigorously derived from the exact microscale data; that is, without introducing any *ad hoc* approximations during the course effecting the requisite

microscale $\rightarrow$ macroscale transition. This is precisely the generic role played by macrotransport theory [12], as exemplified in our model problem, whose details are discussed below.

# Chapter 4

# Macroscale Formulation

An overview of macrotransport theory, together with numerous applications thereof, especially to chromatographic separation phenomena, is presented in the text by Brenner & Edwards [12]. A somewhat more detailed derivation of the generic macroscale formulas appearing therein for analyzing spatially periodic systems, based upon applying a micro/macro moment-matching (homogenization) scheme, is given in several earlier publications [18, 19]. For the purposes of analyzing micropatterned devices, we will present the governing equations formulated exclusively for the case of particle motion induced by a uniform external field and in the absence of bulk fluid motion.[1] This focus departs in a major way from previous analyses [12], which, with a single exception [13], have emphasized solute transport resulting from entrainment of the Brownian tracer in a flowing solvent, and in the absence of external forces. Nevertheless, the requisite analysis required to treat the case of non-convective, force-driven tracer transport already exists, being embodied as a special case within the general theory of macrotransport processes [12, 18, 19].

Macrotransport theory provides a step-by-step paradigm for calculating the macroscale solute velocity vector $\overline{\mathbf{U}}^*$ and dispersivity dyadic $\overline{\mathbf{D}}^*$ appearing in the macroscale convective-

[1] Of course, the resulting flux of Brownian solute particles necessarily produces a mass-average velocity $\mathbf{v}$ when, on average, the solvent remains at rest, as in the present circumstances. However, given the implicit assumption of diluteness, as embodied in our single-particle analysis, this resulting convective velocity $\mathbf{v}$ may be regarded as negligible.

diffusive equation,

$$\frac{\partial \overline{P}}{\partial t} + \overline{\mathbf{U}}^{*} \cdot \nabla \overline{P} = \overline{\mathbf{D}}^{*} : \nabla \nabla \overline{P}, \tag{4.1}$$

governing the unit-cell-averaged, long-time, conditional probability density $\overline{P} = \overline{P}(\mathbf{n}, t; \mathbf{n}_0) \simeq \overline{P}(\mathbf{n} - \mathbf{n}_0; t)$. The latter pertains to the long-time probability that a particle originally introduced anywhere within cell $\mathbf{n}_0$ at time $t = 0$ will be present somewhere within the interior of cell $\mathbf{n}$ at time $t$.[2] Referring to eq. (4.1), $\overline{P}$ satisfies the initial condition

$$\overline{P} = \delta(\mathbf{n} - \mathbf{n}_0) \text{ at } t = 0, \tag{4.2}$$

as well as the fact that

$$\overline{P} \to 0 \text{ as } |\mathbf{n} - \mathbf{n}_0| \to \infty. \tag{4.3}$$

The velocity vector $\overline{\mathbf{U}}^{*}$ appearing in eq. (4.1) is formally defined [12] as the proportionality coefficient appearing in the asymptotic, long-time, Lagrangian trajectory relationship,

$$\overline{\mathbf{R} - \mathbf{R}_0} \equiv \overline{\mathbf{R}} - \mathbf{R}_0 \simeq \overline{\mathbf{U}}^{*} t, \tag{4.4}$$

existing between the mean displacement,

$$\overline{\mathbf{R} - \mathbf{R}_0} \stackrel{\text{def.}}{=} \int_{\mathbf{R}_\infty} (\mathbf{R} - \mathbf{R}_0)\, P(\mathbf{R}; t \,|\, \mathbf{R}_0) d^3\mathbf{R}, \tag{4.5}$$

of the instantaneous position $\mathbf{R}$ of the (center of the) Brownian tracer at time $t$ from its initial position $\mathbf{R}_0$ at time $t$=0. Here, notationally, $d^3\mathbf{R} = dxdydz$ is a volume element, and

$$\int_{\mathbf{R}_\infty} (\cdots)\, d^3\mathbf{R} \equiv \int_{x=-\infty}^{\infty} \int_{y=-\infty}^{\infty} \int_{z=-\infty}^{\infty} (\cdots)\, dxdydz. \tag{4.6}$$

[2]Here, $\mathbf{n} \equiv (n_1, n_2, n_3)$, with $n_k = 0, \pm 1, \pm 2, \ldots$ ; $k = 1, 2, 3$, refers to a trio of integers characterizing the discrete position vector $\mathbf{R_n} = n_1 \mathbf{l}_1 + n_2 \mathbf{l}_2 + n_3 \mathbf{l}_3$ of, say, the centroid of cell $\mathbf{n}$, wherein $(\mathbf{l}_1, \mathbf{l}_2, \mathbf{l}_3)$ denote a trio of basic lattice vectors parameterizing the underlying decomposition of space into space-filling parallelepipedal unit cells [12].

Similarly, the dispersivity dyadic $\overline{\mathbf{D}}^*$ is defined as the proportionality coefficient appearing in the asymptotic, long-time, Einstein-like diffusion relation,

$$\overline{\left(\mathbf{R}-\overline{\mathbf{R}}\right)\left(\mathbf{R}-\overline{\mathbf{R}}\right)} \simeq 2\overline{\mathbf{D}}^* t, \tag{4.7}$$

existing between the mean-squared deviation,

$$\overline{(\mathbf{R}-\overline{\mathbf{R}})(\mathbf{R}-\overline{\mathbf{R}})} \stackrel{\text{def.}}{=} \int_{\mathbf{R}_\infty} d^3\mathbf{R}\,(\mathbf{R}-\overline{\mathbf{R}})(\mathbf{R}-\overline{\mathbf{R}})P(\mathbf{R};t\,|\,\mathbf{R}_0), \tag{4.8}$$

of the instantaneous position $\mathbf{R}$ of the (center of the) Brownian tracer at time $t$ from its mean position $\overline{\mathbf{R}} = \mathbf{R}_0 + \overline{\mathbf{U}}^* t$ at that time. These definitions of $\overline{\mathbf{U}}^*$ and $\overline{\mathbf{D}}^*$ permit both quantities to be computed, at least in principle, from the prescribed microscale data entering into the computation of the fundamental microscale Green's function $P(\mathbf{R};t\,|\,\mathbf{R}_0)$ appearing in the integrands of (4.5) and (4.8). It is this intractable and resource-wasteful microscale calculation of $P(\mathbf{R};t\,|\,\mathbf{R}_0)$ which is replaced by the vastly more feasible scheme for calculating $\overline{\mathbf{U}}^*$ and $\overline{\mathbf{D}}^*$ embodied within macrotransport theory [cf. eqs. (4.12) and (4.21)].

In eq. (4.1), $\overline{P}$ denotes the asymptotic average microscale unit cell solute "concentration" within cell $\mathbf{n}$ at time $t$:

$$\overline{P}(\mathbf{n},t;\mathbf{n}_0) \stackrel{\text{def.}}{\simeq} \frac{1}{\tau_0}\int_{\tau_0\{\mathbf{n}\}} P(\mathbf{R};t\,|\,\mathbf{R}_0)d^3\mathbf{R}, \tag{4.9}$$

where the integration domain $\tau_0\{\mathbf{n}\}$ refers to the interior of cell $\mathbf{n}$.

An important distinction existing between the macrotransport equation (4.1) and its microtransport precursor (3.13) lies in the position-independence of the macrotransport parameters $\overline{\mathbf{U}}^*$ and $\overline{\mathbf{D}}^*$, in contrast with the comparable position-dependent microscale parameters $\mathbf{U}$ and $\mathbf{D}$. As discussed below, calculation of the global macrotransport coefficients $\overline{\mathbf{U}}^*$ and $\overline{\mathbf{D}}^*$ necessitates solving a straightforward, time-independent boundary-value problem posed within a single unit cell. Specifically, as an intermediate step, calculation of these phenomenological coefficients requires detailed microscale solutions for: (i) a certain steady-state, intracell, unconditional probability density $P_0^\infty(\mathbf{r})$ [cf. eqs. (4.13)-(4.19)] for finding the solute particle at a

given position $\mathbf{r} \equiv (x, y, z)$ within the unit cell domain,

$$(\mathbf{r} \in \tau_0) \equiv (0 < x < l_x, 0 < y < l_y, 0 < z < l_z)\,, \tag{4.10}$$

irrespective of its initial global position $\mathbf{R}_0$ (3.8), or of its actual current global cellular position $\mathbf{n}$;[3] and (ii) a so-called intracellular $\mathbf{B}(\mathbf{r})$-field, arising as a consequence of the local particle velocity heterogeneity, $\mathbf{U}(\mathbf{r}) - \overline{\mathbf{U}}^*$, existing at each point within the cell. Fine-scale details of the microscale geometry, viscosity gradient, etc. enter into computation of the intermediate fields $P_0^\infty$ and $\mathbf{B}$, subsequent to which integration of these microscale fields over the unit cell via eqs. (4.12)-(4.13) and (4.21) respectively produces the position-independent macrotransport coefficients $\overline{\mathbf{U}}^*$ and $\overline{\mathbf{D}}^*$. Moreover, the long-time coarse-grained conditional macroscale probability density $\overline{P}$ is dependent only upon the relative *global* or coarse-grained position, $\mathbf{n} - \mathbf{n}_0$, of the solute tracer particle within the current unit cell $\mathbf{n}$ with respect to the original cell $\mathbf{n}_0$, rather than upon the detailed current *local* position, $\mathbf{R} - \mathbf{R}_0$, of $\mathbf{R}$ relative to the initial local position $\mathbf{R}_0$. Equation (4.1), characterized by the constant phenomenological coefficients $\overline{\mathbf{U}}^*$ and $\overline{\mathbf{D}}^*$, lends itself to a vastly simpler solution scheme for calculating $\overline{P}$ than would prove necessary were one to attempt to calculate this quantity directly from the microscale Green's function $P(\mathbf{R}; t\,|\,\mathbf{R}_0)$ via eq. (4.9). As is readily shown, eqs. (4.1)-(4.3) possess the elementary solution

$$\begin{aligned}\overline{P}(\mathbf{n} - \mathbf{n}_0; t) \equiv & \overline{P}(\mathbf{R}_\mathbf{n} - \mathbf{R}_{\mathbf{n}_0}; t) = (4\pi t)^{-3/2} (\det \overline{\mathbf{D}}^*)^{-1/2} \exp[-(4t)^{-1} (\mathbf{R}_\mathbf{n} - \mathbf{R}_{\mathbf{n}_0} - \overline{\mathbf{U}}^* t) \cdot \\ & \cdot (\overline{\mathbf{D}}^*)^{-1} \cdot (\mathbf{R}_\mathbf{n} - \mathbf{R}_{\mathbf{n}_0} - \overline{\mathbf{U}}^* t)]. \end{aligned} \tag{4.11}$$

where $\mathbf{R}_\mathbf{n}$ is described in Note 2.

The phenomenological coefficients $\overline{\mathbf{U}}^*$ and $\overline{\mathbf{D}}^*$ possess the respective Lagrangian interpretations (4.4) and (4.7), different from their conventional Eulerian interpretations in eq. (4.1) as representing coefficients appearing in the respective macroscale solute convective and diffusive fluxes through an arbitrary space-fixed macroscale surface [18]. As discussed, in a

[3] While the original conditional probability density $P$ from which $P_0^\infty$ derives depends upon the initial intracellular location $(x_0, y_0, z_0)$ of the particle, the latter probability density does not. In effect, the particle eventually "forgets" its initial local intracellular starting point after sufficient time has elapsed for it to effectively sample *all* the available points within the cell many times. As such, $P_0^\infty$ is not a *conditional* probability density, but, rather, is unconditional.

Lagrangian context the macroscopic solute velocity and dispersivity represent parameters describing the (stochastic) spatio-temporal trajectory of a given Brownian particle through the micropatterned device. The functional dependencies of $\overline{\mathbf{U}}^*$ (or, more precisely, $\overline{\mathbf{M}}^*$) and $\overline{\mathbf{D}}^*$ upon the process parameters necessarily furnish significant insights into the basic nature of the solute separation process. Specifically, knowledge of the various species-specific solute macroscopic mobility dyadics $\overline{\mathbf{M}}_j^*$ $(j = 1, 2, \dots)$ in a mixture allows one to determine the angular trajectory separation paths pursued by different solute species $j$ possessing differing physical or physiochemical attributes, such as radius $a_j$ and/or physiochemical partition coefficient $K^{(j)}$ in the specified solvents. The species-specific solute dispersivity $\overline{\mathbf{D}}_j^*$ quantifies the degree of band broadening (separation sharpness), an equally important adjunct to $\overline{\mathbf{M}}_j^*$ in the design and interpretation of chromatographic separation devices, but presently incalculable from existing models of the class of micropatterned separation devices [9, 11].

## 4.1 Chromatographic Mobility

The macroscopic solute velocity vector can be computed from knowledge of a certain steady-state probability flux density $\mathbf{J}_0^\infty$ via the quadrature,

$$\overline{\mathbf{U}}^* = \int_{\tau_0} \mathbf{J}_0^\infty(\mathbf{r})\, d^3\mathbf{r}, \tag{4.12}$$

over the unit cell domain $\tau_0$ (4.10) where $d^3\mathbf{r} \equiv dxdydz$ denotes a volume element within the unit cell. In present circumstances, where interstitial solvent convection and, hence, concomitant piggy-back solute convection transport are absent, the flux density $\mathbf{J}_0^\infty$ is given by the expression

$$\mathbf{J}_0^\infty = \mathbf{M} \cdot \mathbf{F}\, P_0^\infty - kT\, \mathbf{M} \cdot \nabla P_0^\infty \qquad (\mathbf{r} \in \tau_0)\,, \tag{4.13}$$

and satisfies the *steady-state* conservation equation

$$\nabla \cdot \mathbf{J}_0^\infty = 0 \tag{4.14}$$

at all points $\mathbf{r} = (x, y, z)$ within the unit cell (4.10).

In combination, eqs. (4.13)-(4.14) furnish a second-order partial differential equation with

a position-dependent mobility coefficient for the field $P_0^\infty(\mathbf{r})$. This intracell probability field is required to satisfy the following "jump" boundary conditions across the external unit cell boundaries $\partial\tau_0$, the latter consisting of the six planar faces ($x$=0, $l_x$), ($y$=0, $l_y$), ($z$=0, $l_z$) bounding the unit cell (4.10):

$$\|P_0^\infty\| = 0, \quad \|\nabla P_0^\infty\| = \mathbf{0} \quad \text{on } \partial\tau_0. \tag{4.15}$$

The jump operator $\|\mathbf{f}\|$ is defined as the difference in the generic tensor field $\mathbf{f}(\mathbf{r})$ between equivalently-situated points lying on each of the three pairs of opposing cell faces. Thus, the jump in the $z$-direction is defined as

$$\|\mathbf{f}\| \stackrel{\text{def.}}{=} \mathbf{f}(x, y, z + l_z) - \mathbf{f}(x, y, z), \tag{4.16}$$

together with similar expressions for the comparable jumps in the $x$- and $y$-directions.

In the presence of a fluid/fluid interface, say $s_p$, separating the two immiscible fluids labeled "1" and "2", and contained within the unit-cell interior, two additional interphase conditions are required in connection with the respective issues of the continuities (or lack thereof) of $\mathbf{J}_0^\infty$ and $P_0^\infty$ across the phase boundary: (i) The assumed absence of surface adsorption at the interface necessitates continuity of the normal component of the solute flux across the interface [cf. eq. (3.16)]:

$$\upsilon\cdot\left[\mathbf{J}_{0(1)}^\infty - \mathbf{J}_{0(2)}^\infty\right] = 0 \quad \text{on } s_p; \tag{4.17}$$

(ii) The assumption of local thermodynamic equilibrium across the interface, as in equation

(3.14), requires that[4]

$$K_1 P_{0(1)}^{\infty} = K_2 P_{0(2)}^{\infty} \quad \text{on } s_p. \tag{4.18}$$

As a final condition imposed on $P_0^{\infty}$, the fact that the (center of the) solute particle must be situated at some local position within the unit cell, together with the original unit impulse initial condition (3.11) necessitates that the present probability density be normalized to unity over a unit cell [12]:

$$\int_{\tau_0} P_0^{\infty} d^3\mathbf{r} = 1. \tag{4.19}$$

Collectively, eq. (4.14) in conjunction with the boundary, interfacial, and normalization conditions (4.15)-(4.19) serve to completely and uniquely define the $P_0^{\infty}$ field within the unit cell interior (4.10). In turn, the resulting knowledge of $P_0^{\infty}$, obtained by solving this system of equations, furnishes the flux density $\mathbf{J}_0^{\infty}$ via eq. (4.13), and ultimately therefrom the macroscale solute velocity via eq. (4.12). As a consequence of the structure of the set of equations (4.12)-(4.19), one need thus only solve relatively simple, unconditional, *steady-state* (microscale) transport equations within the interior of a *single* unit cell in order to obtain $\overline{\mathbf{U}}^*$ (or, equivalently, $\overline{\mathbf{M}}^*$). *Thereby, one is able to completely by-pass having to solve the original unsteady-state, initial-value microscale problem for* $P(\mathbf{R}; t \,|\, \mathbf{R}_0)$ *throughout all space,* $\mathbf{R} \in \mathbf{R}_{\infty}$*, and for all time, posed by equations* (3.13)-(3.16) *in order to obtain* $\overline{\mathbf{U}}^*$ *from eqs.* (4.4)-(4.5)! This fact, in conjunction with a comparable calculation of $\overline{\mathbf{D}}^*$, constitutes the essence of the theory of macrotransport processes [12].

Since solute motion through the micropatterned device is animated solely by the external

[4]In our development we have applied the generic conditions [12] prevailing at interior discontinuities in material properties, if any, to the fluid/fluid interfaces present in our specific physical problem. However, in the more general development of spatially periodic macrotransport theory [12]— particularly more conventional applications involving the presence of solid "obstacles" — interphase boundary conditions such as (4.17) and (4.18) are usually applied at the boundaries between a *continuous* phase and a *discontinuous* phase, the latter representing the obstacles, and the former representing the interstitial fluid phase. In such applications, as for example with real microlithographic arrays, the physical distinction between continuous and discontinuous phases is less equivocal than in the present case, where neither phase is strictly "continuous" in all directions (being continuous in the $x$- and $y$-directions, but discontinuous in the $z$-direction). In any event, in our example, either phase can be arbitrarily designated as constituting the "continuous" phase, since the macrotransport coefficients $\overline{\mathbf{U}}^*$ and $\overline{\mathbf{D}}^*$ ultimately obtained must necessarily prove to be independent of the arbitrary choice of phase labeling, as indeed they do.

force $\mathbf{F}$, in a manner similar to (2.5) it proves convenient to define a (macroscale) chromatographic solute mobility tensor $\overline{\mathbf{M}}^*$ via eq. (1.1). In the context of interpreting separation processes, this chromatographic mobility dyadic proves to be an especially useful physical concept. Were the respective chromatographic species-specific mobility tensors $\overline{\mathbf{M}}_j^*$ found to be isotropic for *all* of the solute species $j$ present in the mixture to be separated, so that $\overline{\mathbf{M}}_j^* = \mathbf{I}\overline{M}_j^*$, the resulting mean species-velocity vectors, $\overline{\mathbf{U}}_j^* = \overline{M}_j^*\mathbf{F}_j$ (where, say,

$$\mathbf{F}_j = \lambda_j \mathbf{E}, \tag{4.20}$$

in which the constant $\lambda_j$ is a species-dependent parameter and $\mathbf{E}$ is the uniform external field giving rise to the force, i.e. an electric field),[5] would then all be colinear with the field $\mathbf{E}$. In such circumstances, the resulting separation scheme would reduce from *vector* chromatography to conventional unidirectional *scalar* chromatography since all species would then move, on average, in the same direction, namely in the direction of the field $\mathbf{E}$. The resulting unidirectional separation process would then depend exclusively upon the respective *speeds* $\left|\overline{\mathbf{U}}_j^*\right|$ of the species, rather than upon the angular trajectory directions, represented, say, by the unit vectors $\overline{\mathbf{U}}_j^* / \left|\overline{\mathbf{U}}_j^*\right| \quad (j = 1, 2, 3, \dots)$, pursued by their respective mean Lagrangian spatio-temporal paths (4.4) through the array of obstacles. However, the ensuing analysis will show, generally, that even when the *local* microscale mobilities $\mathbf{M}_j = \mathbf{I}\,[6\pi\mu(z)a_j]^{-1}$ are isotropic, as in our present layered-fluid example, the resulting chromatographic mobilities $\overline{\mathbf{M}}_j^*$ will, nevertheless, always be anisotropic whenever the point group symmetry class of the combined lattice plus obstacle geometry (the layers in our case) is itself anisotropic with regard to second-rank tensors[6] [20]. In the presence of such anisotropy, and whenever the solutes differ in some pertinent physical or physiochemical attribute serving to distinguish them chromatographically, the distinguished species will generally move in different directions, thereby giving rise to the concept of vector chromatography. Current, *ad hoc* theories of the separation processes in microlitho-

[5]For example, if the Brownian particles were uniformly charged over their surfaces, $\lambda_j$ would then be proportional to the respective surface areas $4\pi a_j$ of the spheres of radius $a_j$, with $\mathbf{F}_j$ proportional to the externally applied electric field $\mathbf{E}$, as in (4.20).

[6]For example, a square lattice containing symmetrically-oriented square obstacles is isotropic with respect to second-rank tensors. On the other hand, were the obstacles rectangular rather than square, the configuration would be anisotropic with respect to second-rank tensors. Indeed, the latter anisotropic configuration was employed by Austin et al. [5] in their pioneering micropatterned device.

graphic arrays [9, 11] do not clearly recognize the generic concept of a macroscale mobility tensor. As such, these theories necessarily fail to capture the fundamental anisotropy of the vector chromatographic separation scheme, although, of course, this anisotropy is fundamental to the micropatterned separation process itself, as implicitly recognized by the inventors of this novel process [9, 11].

## 4.2 Dispersivity

The macroscopic solute dispersivity, which differs fundamentally from that of a simple coarse-grained average of the solute's microscale diffusivity $\mathbf{D}$ (that is, its "hindered" *molecular* diffusivity[7]), can be calculated by effecting the following unit cell quadrature:

$$\overline{\mathbf{D}}^{*} = \int_{\tau_0} P_0^{\infty} \left(\nabla \mathbf{B}\right)^{\dagger} \cdot \mathbf{D} \cdot \nabla \mathbf{B} d^3\mathbf{r}, \tag{4.21}$$

where † denotes the transposition operator. The generic equation defining the steady-state field $\mathbf{B}(\mathbf{r})$ required above is

$$\nabla \cdot (P_0^{\infty} \mathbf{D} \cdot \nabla \mathbf{B}) - \mathbf{J}_0^{\infty} \cdot \nabla \mathbf{B} = P_0^{\infty} \overline{\mathbf{U}}^{*} \quad (\mathbf{r} \in \tau_0)\,. \tag{4.22}$$

This equation is to be solved subject to the following jump conditions across the unit cell boundaries:

$$\|\mathbf{B}\| = -\|\mathbf{r}\|\,, \quad \|\nabla \mathbf{B}\| = \mathbf{0} \quad \text{on } \partial\tau_0, \tag{4.23}$$

where $\mathbf{r} = \mathbf{i}_x x + \mathbf{i}_y y + \mathbf{i}_z z$ denotes the local position vector of a point within the cell.

For the present immiscible layered-fluid case, two internal conditions are imposed upon the $\mathbf{B}$-field at the phase interface $s_p$ existing within the unit cell interior:[8] (i) The assumption of

[7] "Hindered" molecular diffusivity refers, in general, to the fact that the interstitial- or pore-level molecular diffusivity of the *center* of the Brownian sphere is locally affected by the proximity of the sphere to the surfaces of the obstacles comprising the micropatterned device. Accordingly, the (generally anisotropic) hindered molecular diffusivity $\mathbf{D}$, which generally includes such hydrodynamic wall effects, will vary locally with the sphere's microscale position within the unit cell. This diffusivity can be calculated from a Stokes-Einstein relation, $\mathbf{D} = kT\mathbf{M}$, where the (Stokes) mobility tensor $\mathbf{M}$ is to be calculated by taking account of hydrodynamic wall effects [21, 22].

[8] Again, in this example the interphase conditions are applied at the *fluid-fluid* interface, whereas such con-

local thermodynamic equilibrium at the interface requires that

$$\mathbf{B} \text{ is continuous across } s_p; \tag{4.24}$$

and (ii) from the required continuity (3.16) of the normal component of the solute flux across the interface,

$$\upsilon \cdot \left[ P^{\infty}_{0(1)} \mathbf{D}_{(1)} \cdot \nabla \mathbf{B}_{(1)} - P^{\infty}_{0(2)} \mathbf{D}_{(2)} \cdot \nabla \mathbf{B}_{(2)} \right] = 0 \text{ on } s_p. \tag{4.25}$$

The governing transport equation (4.22) together with the boundary and continuity conditions (4.23)-(4.25) serves to uniquely define the $\mathbf{B}$ field within the unit cell, albeit only to within an arbitrary additive constant vector. As the calculation of $\overline{\mathbf{D}}^*$ from (4.21) requires knowledge only of $\nabla \mathbf{B}$ rather than $\mathbf{B}$ itself, this lack of uniqueness is without physical consequence.

## 4.3 Macroscale Solution

Having presented in the previous section the relevant microscale equations governing $P^{\infty}_0$ and $\mathbf{B}$, which enter into the calculations of $\overline{\mathbf{M}}^*$ and $\overline{\mathbf{D}}^*$, we proceed now to solve these unit cell microscale equations for the two closely-related variable viscosity problems described earlier: (i) initially for a general periodic viscosity function which is continuous everywhere within the unit cell $\tau_0$ (so that no internal interface $s_p$ exists); and (ii) subsequently for the specific discontinuous viscosity case, where two immiscible fluid layers, each of uniform viscosity, exist within the unit cell, and hence for which the presence of the interior interface $s_p$ within the unit cell must be explicitly recognized via the interface boundary conditions (4.17)-(4.18) relevant to $P^{\infty}_0$ and those relevant to $\mathbf{B}$, namely (4.24)-(4.25).

Due to the spatial periodicity of the microscale geometry, the coordinate system $(x, y, z)$ defined within the interior of the unit cell can be drawn with respect to an origin chosen to lie at some arbitrary point, say $z'$ $(-\infty < z' < \infty)$, with the corresponding local $z$-position within a cell written as $z - z'$ relative to this choice of origin, in which $z = 0$ and $z = l_z$

ditions are more generically applied at the *solid-fluid* interface existing between the respective "discontinuous" and "continuous" phases [12] when solid obstacles are present.

respectively identify the unit cell boundaries. Use of this notation serves to highlight, *inter alia*, the independence of the final physical results from the arbitrary choice of origin. Since the characteristic length of the unit cell is the viscosity period $l_z$, it proves convenient to introduce a dimensionless axial coordinate:

$$z^* \stackrel{\text{def.}}{=} \frac{z - z'}{l_z}, \tag{4.26}$$

so that $0 < z^* < 1$ within the unit cell. Rather than carry along the asterisk affixed to $z$ throughout the subsequent analysis, we will, for notational simplicity, suppress it in what follows, albeit at the risk of some slight confusion. However, it will always be obvious from the context of the discussion to which of the two $z$'s, physical or dimensionless, reference is being made.

# Chapter 5

# Chromatographic Mobility

## 5.1 Continuous Periodic Viscosity Case

### 5.1.1 Calculation of $P_0^\infty$

Assume, subject to *a posteriori* verification, that the intracell solution $P_0^\infty(\mathbf{r})$ of the preceding system of equations is of the form $P_0^\infty(z)$, independently of $x$ and $y$. Equation (4.13) thereby reduces to

$$\mathbf{J}_0^\infty = \frac{1}{6\pi a}\left[\mathbf{F}\frac{P_0^\infty(z)}{\mu(z)} - \mathbf{i}_z kT\frac{1}{\mu(z)}\frac{dP_0^\infty(z)}{dz}\right] \ (0 < z < 1)\,, \tag{5.1}$$

where the external force vector $\mathbf{F}$ possesses the respective components noted in (1.2). As a consequence of (4.14), the following second-order ordinary differential equation obtains for $P_0^\infty(z)$:

$$\frac{d}{dz}\left[\frac{1}{\mu(z)}\frac{dP_0^\infty(z)}{dz}\right] - \mathrm{Pe}\frac{d}{dz}\left[\frac{P_0^\infty(z)}{\mu(z)}\right] = 0 \quad (0 < z < 1), \tag{5.2}$$

with Pe the longitudinal (or axial) Peclet number defined on the viscosity period:

$$\mathrm{Pe} = \frac{F_z l_z}{kT}. \tag{5.3}$$

Integrate (5.2) twice to obtain the general solution

$$P_0^\infty(z) = -C\,\mathrm{Pe}\exp(\mathrm{Pe}\,z)\left[P_0^\infty(0) + \int_0^z dz'\mu(z')\exp\left(-\mathrm{Pe}\,z'\right)\right], \tag{5.4}$$

with $C$ and $P_0^\infty(0)$ integration constants to be determined from the unit cell boundary and normalization conditions. From the first of the two jump conditions (4.15), which reduces in present circumstances to the requirement that $P_0^\infty(z=1) = P_0^\infty(z=0)$, we find for the value of the constant $P_0^\infty(0)$ that

$$P_0^\infty(0) = \frac{\exp(\mathrm{Pe})\int_0^1 dz\,\mu(z)\exp(-\mathrm{Pe}\,z)}{1-\exp(\mathrm{Pe})}. \tag{5.5}$$

Substitution of (5.4) and (5.5) into the second of the requisite jump conditions (4.15), namely $(dP_0^\infty/dz)_{z=1} = (dP_0^\infty/dz)_{z=0}$, reveals that this jump condition is automatically satisfied by the solution (5.4) for any choice of the constant $C$.

Normalization of (5.4) in accordance with (4.19) provides the remaining constant $C$:

$$\begin{aligned}\frac{C^{-1}}{\tau_0} &= \exp(\mathrm{Pe})\int_0^1 dz\,\mu(z)\exp(-\mathrm{Pe}\,z) - \\ &\quad - \mathrm{Pe}\int_0^1 dz\exp(\mathrm{Pe}\,z)\int_0^z dz'\mu(z')\exp\left(-\mathrm{Pe}\,z'\right)\end{aligned} \tag{5.6}$$

Knowledge of the constants $C$ and $P_0^\infty(0)$ appearing in (5.4) furnishes the field $P_0^\infty$, as well as the flux $\mathbf{J}_0^\infty$ from eq. (5.1). Inasmuch as the solution obtained for $P_0^\infty$ satisfies all of the requisite conditions demanded of it, this justifies *a posteriori* our assumption that $P_0^\infty$ is independent of $x$ and $y$.

### 5.1.2 Calculation of $\overline{\mathbf{M}}^*$

The macroscopic velocity $\overline{\mathbf{U}}^*$ is functionally related to the flux $\mathbf{J}_0^\infty$ by the generic equation (4.12). In conjunction with the definition (1.1) of the chromatographic mobility, the latter is

thereby found to be of the form

$$\overline{\mathbf{M}}^* = \mathbf{i}_z\mathbf{i}_z\overline{M}^*_\perp + (\mathbf{I} - \mathbf{i}_z\mathbf{i}_z)\,\overline{M}^*_\parallel, \tag{5.7}$$

wherein

$$\overline{M}^*_\perp = \frac{\tau_o}{6\pi a}C, \qquad \overline{M}^*_\parallel = \frac{\tau_o}{6\pi a}\int_0^1 dz\frac{P_0^\infty(z)}{\mu(z)}. \tag{5.8}$$

The chromatographic mobility dyadic $\overline{\mathbf{M}}^*$ is thus seen to be transversely isotropic with respect to the direction $z$ of the viscosity gradient, as would be expected based upon intuitive geometric symmetry considerations.[1] The integrand of the perpendicular mobility component, corresponding to the first of equations (5.8), possesses the generic interpretation of arising from "resistances in series" since $C$ [see (5.6)] involves the viscosity function $\mu(z)$ appearing in the numerator of the integrand. Conversely, the parallel mobility component, corresponding to the second of equations (5.8), possesses, as a result of the presence of the viscosity function $\mu(z)$ in the denominator, the elementary physical interpretation of arising from "resistances in parallel" (bearing in mind that the weighting function $P_0^\infty$ is probabilistic, rather than geometrical).

### 5.1.3 Sinusoidal Viscosity Function

As a simple example of this genre, consider a periodic viscosity field of the form

$$\mu(z) = \mu_0\left[1 + \alpha^{-1}\sin(2\pi z)\right] \qquad (0 < z < 1), \tag{5.9}$$

where $\alpha > 1$ is a constant, with the latter inequality chosen to assure that the viscosity is non-negative everywhere. The constant $\mu_0$ represents an average or macroscale viscosity, whereas $\alpha$ quantifies the degree of inhomogeneity of the periodic viscosity field, with $\alpha \to \infty$ corresponding to a homogeneous fluid of uniform viscosity $\mu_0$. The microscale viscosity field (5.9) possesses identical values on each of the two faces $z$=(0, 1) of the unit cell, thus guaranteeing its periodicity

[1] In the physically uninteresting case where $\mu$ is a constant, independent of $z$, it is readily confirmed, as would be expected, that the resulting chromatographic mobility $\overline{\mathbf{M}}^*$ is isotropic, and is, in fact, identical to the *microscale* Stokes mobility $\mathbf{M}$, given in eq. (2.6a).

throughout all of space ($-\infty < z < \infty$). Extensive algebraic manipulations eventually yield the mobility components

$$\overline{M}_{\perp}^{*} = \frac{1}{6\pi\mu_0 a}, \quad \overline{M}_{\parallel}^{*} = \frac{\beta(\alpha, \mathrm{Pe})}{6\pi\mu_0 a}, \tag{5.10}$$

in which

$$\beta = \mathrm{Pe} \int_0^1 dz \frac{\exp(\mathrm{Pe}\, z)}{1 + \alpha^{-1}\sin(2\pi z)} \left[ \frac{\exp(\mathrm{Pe})}{\exp(\mathrm{Pe}) - 1} \int_0^1 dz\, \gamma(z) - \int_0^z dz' \gamma(z') \right], \tag{5.11}$$

with the function $\gamma(z)$ defined as

$$\gamma(z) = \exp(-\mathrm{Pe}\, z) \left[ 1 + \alpha^{-1}\sin(2\pi z) \right]. \tag{5.12}$$

Thus, despite the fact that the microscale mobility dyadic $\mathbf{M}$ is isotropic, the chromatographic mobility dyadic $\overline{\mathbf{M}}^{*}$, given by (5.7), is anisotropic owing to the deviation of the factor $\beta$ appearing in (5.10) from unity (see Fig. 3). The dependence of $\overline{M}_{\perp}^{*}$ upon the average viscosity $\mu_0$ corresponds in its consequences to an infinite sequence of infinitesimally thin resistances in series,[2] whereas the dependence of $\overline{M}_{\parallel}^{*}$ upon the longitudinal Peclet number Pe is a consequence of the dependence of the probabilistic weighting factor $P_0^{\infty}$ upon Pe. It is easily verified, as expected, that $\beta = 1$ in the zero-valued axial force limit, $\mathbf{F} = \mathbf{0}$ (for which Pe=0), in which circumstances the chromatographic mobility reduces to its expected isotropic, purely molecular, Stokes-Einstein value based upon the mean viscosity $\mu_0$, namely $\overline{\mathbf{M}}^{*} \equiv \mathbf{M} = \mathbf{I}\,(6\pi\mu_0 a)^{-1}$.

Even for the simple sinusoidal viscosity choice (5.9), $\overline{M}_{\parallel}^{*}$ does not possess a closed-form representation [since the integration of eq. (5.11) cannot be effected analytically], underscoring the eventual necessity for purely numerical solutions in the comparable analysis of more geometrically realistic micropatterned devices. Figure 5-1 presents results obtained numerically for $\beta$ as a function of the inhomogeneity parameter $\alpha$ at several longitudinal Peclet numbers. Regardless of Peclet number, $\beta$ eventually attains an asymptotic value of unity as $\alpha$ increases,

[2] In the series direction, namely $z$, the particle can be envisioned as translating through an infinite sequence of infintesimally thin "layers," where each layer locally possesses a uniform viscosity $\mu(z)$. Accordingly, the viscosity integrand appearing in eq. (5.6) is physically equivalent to the conventional definition of resistances in series.

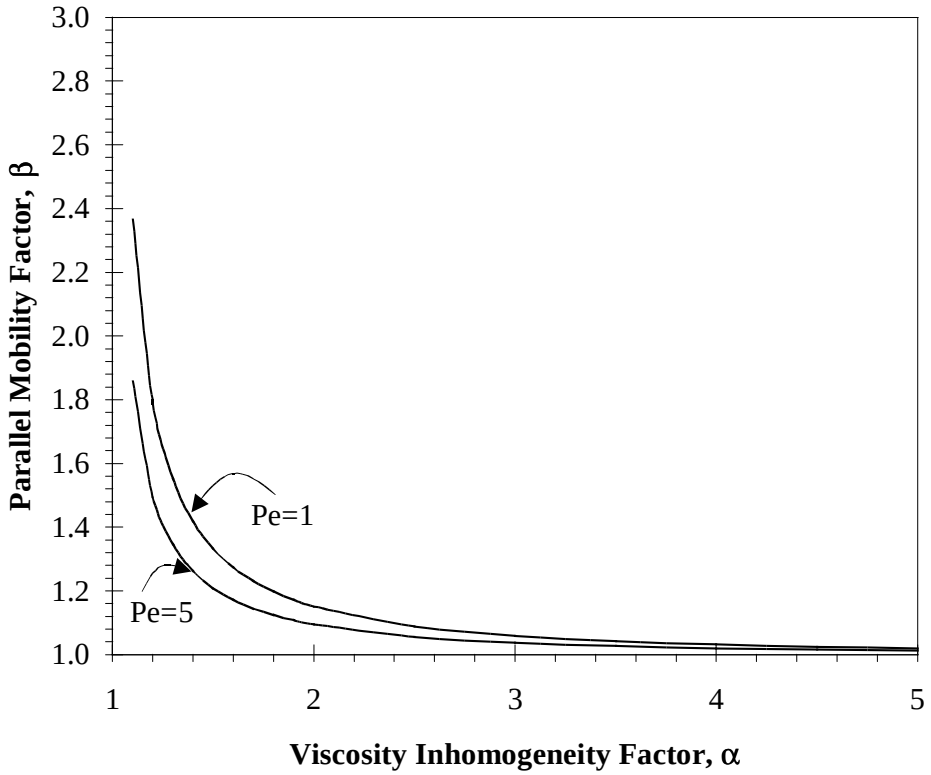


Figure 5-1: Parallel mobility factor $\beta$ as a function of the viscosity inhomogeneity factor $\alpha$ for several longitudinal Peclet numbers.

corresponding to a monotonically increasing degree of homogeneity of the viscosity field with increasing $\alpha$. In the limit $\alpha \to \infty$ the viscosity field becomes completely homogeneous, whence the isotropic Stokes law microscale mobility value ($\beta = 1$) is attained for the macroscale chromatographic mobility as well. The numerical results in Fig. 5-1 bear out the expectation that the mobility factor $\beta$ decreases with increasing Peclet number (thereby diminishing the effect of the Brownian motion relative to that of the external force) – a consequence of the fact that Stokes law does not incorporate Brownian motion effects. In the aphysical limit, $\alpha = 1$ (corresponding to a fluid whose viscosity vanishes at some point within the interior of the unit cell), we recover the equally implausible limit, $\overline{M}^*_{\parallel} \to \infty$. This latter, purely mathematical result is to be expected since, as discussed, $\overline{M}^*_{\parallel}$ arises from resistances in parallel and, in this $\alpha = 1$ limit, a "layer" exists within the unit cell manifesting a vanishing viscosity, zero hydrodynamic resistance limit, thereby furnishing an effectively infinite mobility!

## 5.2 Immiscible Layered Case

Similar to the results obtained above for the preceding, continuously-varying periodic viscosity case, it is relatively straightforward to calculate the comparable chromatographic mobility components, $\overline{M}^*_{\perp}$ and $\overline{M}^*_{\parallel}$, for the case of alternating layers of immiscible fluids, albeit algebraically complicated by the fact that one must now satisfy the additional conditions (4.17)-(4.18) at the phase interface $s_p$. Defined on the dimensionless coordinate system (4.26), with origin $z'$ chosen for convenience to coincide with the internal fluid interface $s_p$, the viscosity function within the unit cell domain, $(0 < z < 1)$, is taken to be of the piecewise constant form [cf. (2.3)]:

$$\mu(z) = \begin{cases} \mu_1 = \text{const.} & (0 < z < \epsilon_1)\,, \\ \mu_2 = \text{const.} & (\epsilon_1 < z < 1)\,. \end{cases} \tag{5.13}$$

### 5.2.1 Calculation of $P_0^\infty$

Assume, subject to *a posteriori* verification, that the intracellular solution $P_0^\infty$ possesses the following piecewise discontinuous form:

$$P_0^\infty(z) = \begin{cases} P_{0(1)}^\infty(z) & (0 < z < \epsilon_1)\,, \\ P_{0(2)}^\infty(z) & (\epsilon_1 < z < 1)\,, \end{cases} \tag{5.14}$$

wherein

$$\begin{aligned} P_{0(1)}^\infty(z) &= \hat{C}\mu_1 + \exp(\mathrm{Pe}\, z)\left[P_{0(1)}^\infty(0) - \hat{C}\mu_1\right], \\ P_{0(2)}^\infty(z) &= \hat{C}\mu_2 + \exp(\mathrm{Pe}\, z)\left[\begin{array}{l} -\hat{C}\mu_2 \exp(-\mathrm{Pe}\,\epsilon_1) + \\ +\dfrac{K_1}{K_2}\left\{\begin{array}{l} -\hat{C}\mu_1\left[1 - \exp(-\mathrm{Pe}\,\epsilon_1)\right] + \\ +P_{0(1)}^\infty(0) \end{array}\right\} \end{array}\right], \end{aligned} \tag{5.15}$$

with $\hat{C}$ and $P_{0(1)}^\infty(0)$ constants to be determined. This solution automatically satisfies the governing differential equation (4.14) piecewise, as well as the flux continuity condition (4.17) and the phase partition condition (4.18), both occurring at $z = \epsilon_1$. Thus, it remains only to satisfy the pair of jump boundary conditions (4.15), as well as the normalization condition (4.19).

Since, with our choice of coordinates a transition occurs in physiochemical solute-solvent properties on the two faces $z$=$(0, 1)$ of the unit cell, the first of the jump conditions (4.15), namely $P_{0(1)}^\infty(0) = P_{0(2)}^\infty(1)$, is replaced with a combination "jump/interface" condition:

$$K_1 P_{0(1)}^\infty(0) = K_2 P_{0(2)}^\infty(1), \tag{5.16}$$

whereby one obtains the value of the constant[3]

$$P^{\infty}_{0(1)}(0) = \frac{\hat{C}}{K_1\left[1-\exp\left(\mathrm{Pe}\right)\right]}\left\{\begin{array}{l} K_2\mu_2\left[\exp\left(\mathrm{Pe}\,\epsilon_2\right)-1\right]- \\ -K_1\mu_1\left[\exp\left(\mathrm{Pe}\right)-\exp\left(\mathrm{Pe}\,\epsilon_2\right)\right] \end{array}\right\}. \tag{5.17}$$

In obtaining the latter, we have made use of the relationship $\epsilon_1 + \epsilon_2 = 1$.

From the normalization condition (4.19) it follows that the remaining constant is given by the expression

$$\hat{C}^{-1} = \tau_0\left(\mu_1\epsilon_1 + \mu_2\epsilon_2 + K'\right), \tag{5.18}$$

wherein

$$K' = -\frac{\left[1-\exp\left(\mathrm{Pe}\,\epsilon_1\right)\right]\left[1-\exp\left(\mathrm{Pe}\,\epsilon_2\right)\right]}{\mathrm{Pe}\left[1-\exp\left(\mathrm{Pe}\right)\right]}\left[\mu_1\left(\frac{K_1}{K_2}-1\right)+\mu_2\left(\frac{K_2}{K_1}-1\right)\right]. \tag{5.19}$$

The respective probability densities within each phase are thereby obtained as[4]

$$\begin{aligned} P^{\infty}_{0(1)}(z) &= \mu_1\hat{C}\left\{1-\exp\left(\mathrm{Pe}\,z\right)\left[\frac{1-\exp\left(\mathrm{Pe}\,\epsilon_2\right)}{1-\exp\left(\mathrm{Pe}\right)}\right]\left(1-\frac{K_2\mu_2}{K_1\mu_1}\right)\right\}, \\ P^{\infty}_{0(2)}(z) &= \mu_2\hat{C}\left\{1-\exp\left(\mathrm{Pe}\,z\right)\left[\frac{1-\exp\left(-\mathrm{Pe}\,\epsilon_1\right)}{1-\exp\left(\mathrm{Pe}\right)}\right]\left(\frac{K_1\mu_1}{K_2\mu_2}-1\right)\right\}. \end{aligned} \tag{5.20}$$

That equations (5.20) satisfy, piecewise, the governing differential equation as well as the requisite auxiliary conditions justifies *a posteriori* our assumption (5.15) for the trial-solution form of $P^{\infty}_0$.

In the effectively zero-force, dominant Brownian motion limit, Pe=0, the respective proba-

[3]Unlike the continuous viscosity case, the solution for $P^{\infty}_0(z)$ does not automatically satisfy the jump condition $\|\nabla P^{\infty}_0\| = \mathbf{0}$ on $\partial\tau_0$ as a consequence of having satisfied the condition $\|P^{\infty}_0\| = 0$. This is due solely to our (arbitrary) choice of the location of the boundaries $\partial\tau_0$ of the unit cell as coinciding with the phase interface(s) $s_p$. It can be verified, albeit with significantly more algebraic effort, that identical results obtain for $\overline{\mathbf{U}}^*$ by choosing a unit cell for which this coincidence is avoided; that is, where the $z$-face boundaries of the unit cell lie wholly within the interior of either fluid "1" or fluid "2."

[4]The apparent lack of interchangability between the arbitrarily-chosen index labels "1" and "2" appearing in the pair of equations (5.20) may be rectified by defining a more "egalitarian" axial coordinate, say $\widetilde{z}$, for phase "2", such that $\widetilde{z} = z + \epsilon_1$.

bility densities (5.20) reduce to

$$P^{\infty}_{0(1)}(z) = C_d, \quad P^{\infty}_{0(2)}(z) = \frac{K_1}{K_2} C_d, \tag{5.21}$$

wherein

$$C_d^{-1} = \tau_0 \left( \epsilon_1 + \frac{K_1}{K_2} \epsilon_2 \right). \tag{5.22}$$

Equations (5.21)-(5.22) accord with existing results [12] for the pure diffusion (force-free) case in layered media.

### 5.2.2 Calculation of $\overline{M}^*_\perp$

Equation (5.8) for the perpendicular chromatographic mobility component explicitly yields

$$\overline{M}^*_\perp = \frac{1}{6\pi\mu_\perp a}, \tag{5.23}$$

in which the effective "perpendicular" viscosity, $\mu_\perp$, is defined as

$$\mu_\perp \stackrel{\text{def.}}{=} \mu_1\epsilon_1 + \mu_2\epsilon_2 + K'. \tag{5.24}$$

This expression for the axial mobility coefficient is independent of the arbitrary choices made for both phase labels and coordinate origin, as must necessarily be the case on purely physical grounds.

Figure 5-2 depicts the functional dependence of $\mu_\perp$ (normalized with the "series" viscosity, $\mu_1\epsilon_1 + \mu_2\epsilon_2$) upon $K$ for the case where $\mu_1/\mu_2 = 0.6$ and $\epsilon_1 = 0.3$, and for two different longitudinal Peclet numbers.[5] These values for $\mu_1/\mu_2$ and $\epsilon_1$ were chosen arbitrarily; other parametric choices would simply have explored the series-like properties of the effective perpendicular viscosity. It is readily shown in the equal partitioning limit ($K \equiv K_1/K_2 = 1$), or when Pe $\to \infty$, that $\mu_\perp$ may be interpreted as arising from resistances in series (represented by a value

[5] Limiting $K$ to the range $0 \leq K \leq 1$ completely explores the variable phase space since: (i) $K$ is non-negative; and (ii) the independence of the macrotransport parameters from the arbitary choice of phase labels necessitates that physical situations in which $K > 1$ are described by the dual problem wherein the indices "1" and "2" are interchanged wherever they appear.

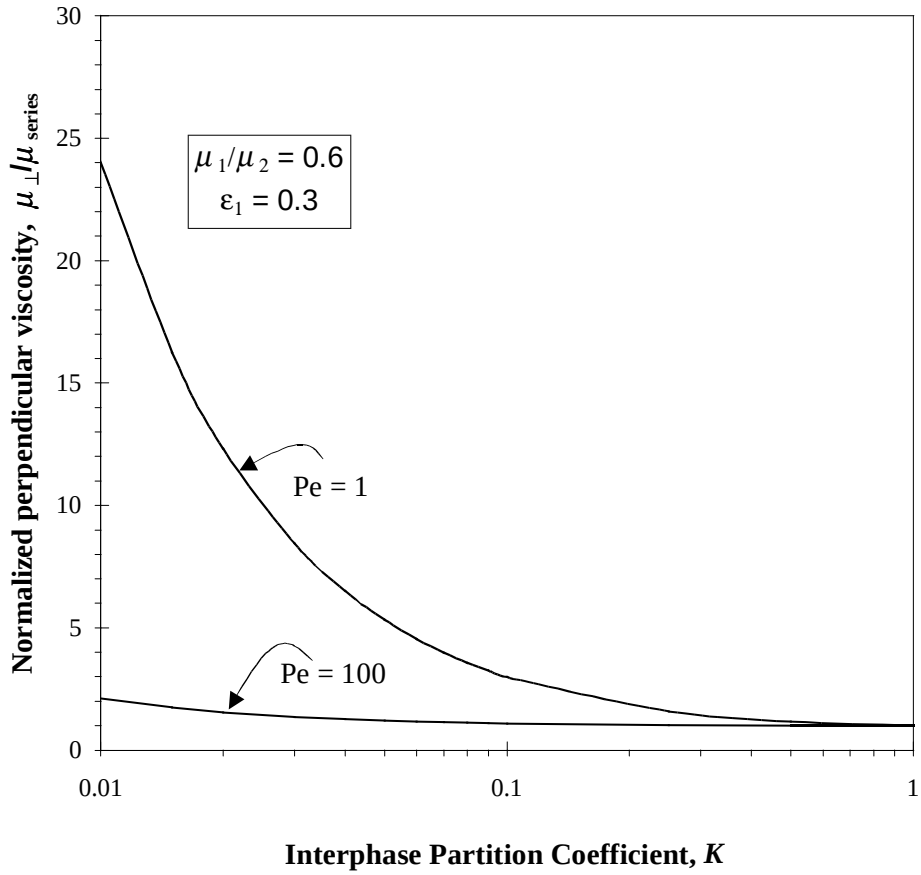


Figure 5-2: Dependence of the effective perpendicular viscosity $\mu_\perp$ (normalized with the "series" viscosity, $\mu_{\text{series}} \stackrel{\text{def.}}{=} \mu_1\epsilon_1 + \mu_2\epsilon_2$ ) upon the thermodynamic partition coefficient $K$, for the fixed phase viscosity ratio and layer volume fraction shown in the inset, and for several longitudinal Peclet numbers.

of unity along the abscissa of Fig. 5-2); that is, in this limit $\mu_\perp$ represents a linear composite of hydrodynamic resistances to transit by the sphere across each fluid layer [see eq. (7.6)]. The case of unequal solute partitioning across the interface introduces an additional contribution to the perpendicular solute concentration gradient, thereby enhancing the molecular diffusion contribution to the total solute flux $\mathbf{J}_0^\infty$ appearing in eq. (4.13) as subsequently discussed in connection with eq. (7.6). In circumstances where Pe$\rightarrow\infty$, thereby rendering diffusion effects negligible, this additional gradient does not contribute to the flux.

In the dominant Brownian motion limit, Pe=0, the perpendicular viscosity coefficient reduces to

$$\lim_{\mathrm{Pe}\rightarrow 0} \mu_\perp = \frac{(K_2\epsilon_1 + K_1\epsilon_2)}{K_1 K_2}\left(K_1\mu_1\epsilon_1 + K_2\mu_2\epsilon_2\right). \tag{5.25}$$

Upon scalarly multiplying the chromatographic mobility (5.23) implied by the latter viscosity coefficient with the zero-valued force, $\mathbf{F} = \mathbf{0}$, corresponding to the pure diffusion, Pe=0, case, one confirms from eq. (1.1) the obvious fact that $\overline{\mathbf{U}}^* = \mathbf{0}$ in this limiting case.

The limiting value $\mu_\perp = \infty$ arises in two distinct circumstances, namely when either $\mu_1 \rightarrow \infty$ (or, equivalently, $\mu_2 \rightarrow \infty$), or when the Brownian solute particle is excluded from one of the two phases by virtue of a zero-valued partition coefficient, $K_1 = 0$ or $K_2 = 0$. Finally, when the two layers possess identical viscosities, but either one (or both) of the solute-solvent systems is nonideal (so that $K_1/K_2 \neq 1$), $K'$ is non-zero, thereby confirming our previous assertion that the case where $\mu_1 = \mu_2 = \text{const.} = \mu$, say, does not necessarily correspond to the case of a rheologically (and thermodynamically) homogeneous fluid of uniform viscosity $\mu$.

### 5.2.3 Calculation of $\overline{M}_\parallel^*$

The parallel mobility component $\overline{M}_\parallel^*$ may be obtained via piecewise integration of the second of equations (5.8). Expressing the parallel mobility in a linear, Stokes-like mobility form, the effective "parallel" viscosity $\mu_\parallel$, defined by the relation

$$\overline{M}_\parallel^* = \frac{1}{6\pi\mu_\parallel a}, \tag{5.26}$$

is given by the expression

$$\mu_{\parallel} \stackrel{\text{def.}}{=} \frac{\mu_1\epsilon_1 + \mu_2\epsilon_2 + K'}{\left\{ \begin{array}{l} 1 + \dfrac{\left[1-\exp(\mathrm{Pe}\,\epsilon_1)\right]\left[1-\exp(\mathrm{Pe}\,\epsilon_2)\right]}{\mathrm{Pe}\left[1-\exp(\mathrm{Pe})\right]} \times \\ \times \left(2 - \dfrac{K_2\mu_2}{K_1\mu_1} - \dfrac{K_1\mu_1}{K_2\mu_2}\right) \end{array} \right\}}. \tag{5.27}$$

Like its perpendicular counterpart, this effective viscosity "component" is invariant to the arbitrary choice of phase labels, as well as to the location of the unit cell $z$-coordinate origin.

Although the parallel component viscosity formula (5.27) does not readily lend itself to interpretation as representing resistances in parallel, it nevertheless retains many of the same attributes. For example, when $\mu_1 \to \infty$ one has that $\mu_{\parallel} = \mu_2$. When $\mu_1 \to 0$ it follows that $\mu_{\parallel} \to 0$. In the infinite partitioning limit, say where $K_1 = 0$, thereby excluding the solute from phase 2, it is found that $\mu_{\parallel} = \mu_1$.

Inasmuch as many of the essential qualitative features possessed by $\mu_{\parallel}$ are already embodied in our discussion of parallel-like resistances in the preceding paragraph, a graphical display of $\mu_{\parallel}$ for various values of Pe and $K$ would reveal minimal new information. As such, no parametric plot of $\mu_{\parallel}$ is presented here. Rather, more significant insights arise upon examining simple limiting cases of the analytical solution (5.27). For example, when solute is equally partitioned between the two phases (corresponding to the ideal fluid case $K = 1$), one finds that

$$\lim_{K\to 1} \mu_{\parallel} = \frac{\mu_1\epsilon_1 + \mu_2\epsilon_2}{\left\{ \begin{array}{l} 1 - \dfrac{\left[1-\exp(\mathrm{Pe}\,\epsilon_1)\right]\left[1-\exp(\mathrm{Pe}\,\epsilon_2)\right]}{\mathrm{Pe}\left[1-\exp(\mathrm{Pe})\right]} \times \\ \times \dfrac{(\mu_1-\mu_2)^2}{\mu_1\mu_2} \end{array} \right\}}. \tag{5.28}$$

The exponential longitudinal Peclet number functions appearing above, absent in the comparable equi-partitioned perpendicular viscosity case [see (5.24), where $K' = 0$], reflect the probabilistic weighting effects appearing in the parallel chromatographic mobility expression (5.27). In the limit where $\mu_1 = \mu_2 = \text{const.} = \mu$, say, and $K_1 = K_2$, it is found that $\mu_{\parallel} = \mu$. Conversely in this same equal viscosity limiting case, $\mu_{\parallel} \neq \mu$ whenever $K_1 \neq K_2$ (corresponding to unequal partitioning), again confirming our assertion that the case of identical, uniform viscosity fluid, albeit forming non-ideal solutions with the solute, is distinct from that for a

rheologically homogeneous fluid of viscosity $\mu$.

Finally, the limiting, dominant Brownian motion, effectively force-free expression,

$$\lim_{\mathrm{Pe}\to 0} \mu_{\parallel} = \frac{\mu_1 \mu_2 \left(K_2 \epsilon_1 + K_1 \epsilon_2\right)}{\mu_1 K_1 \epsilon_2 + \mu_2 K_2 \epsilon_1}, \tag{5.29}$$

reduces to a manifestation of resistances in parallel in the $K_1 = K_2$ limit of equal partitioning.

### 5.2.4 Angular Separation

In order to render explicit, via eqs. (1.1) and (5.8), the angular separation existing between solute species possessing differing physical properties, it is convenient to decompose the vector force $\mathbf{F}$ into components along the axial direction $z$ and transverse to it:

$$\mathbf{F} = \mathbf{i}_z F_z + \mathbf{i}_{\parallel} F_{\parallel}, \tag{5.30}$$

where $F_z = \mathbf{i}_z \cdot \mathbf{F} \geq 0$ is the force component in the $z$-direction, and

$$F_{\parallel} \stackrel{\text{def.}}{=} \left(|\mathbf{F}|^2 - F_z^2\right)^{1/2} \geq 0 \tag{5.31}$$

is the transverse component of the force. Here, $\mathbf{i}_{\parallel}$ is the unit vector

$$\mathbf{i}_{\parallel} \stackrel{\text{def.}}{=} \frac{\mathbf{F} - \mathbf{i}_z F_z}{F_{\parallel}}, \tag{5.32}$$

lying in the transverse $x$-$y$ plane, normal to $\mathbf{i}_z$.

Upon expressing the macroscopic velocity vector in the component form

$$\overline{\mathbf{U}}^* = \mathbf{i}_z \overline{U}_z^* + \mathbf{i}_{\parallel} \overline{U}_{\parallel}^*, \tag{5.33}$$

we find from eqs. (1.1), (5.7) and (5.30) that

$$\overline{U}_z^* = \overline{M}_{\perp}^* F_z, \qquad \overline{U}_{\parallel}^* = \overline{M}_{\parallel}^* F_{\parallel}. \tag{5.34}$$

Thus, if $\theta$ $(0 \leq \theta \leq 90^\circ)$ denotes the angle made with the $z$-axis by the (linear) macroscale

solute trajectory (4.4), we have by definition that

$$\tan\theta = \frac{\overline{U}^*_{\parallel}}{\overline{U}^*_z} \equiv \frac{\overline{M}^*_{\parallel} F_{\parallel}}{\overline{M}^*_{\perp} F_z} \quad (0 \leq \theta \leq 90^\circ)\,. \tag{5.35}$$

Using the relation (4.20), eq. (5.35) yields, for the chromatographic trajectory angle $\theta_j$ of species $j$,

$$\tan\theta_j = \frac{\overline{M}^{*(j)}_{\parallel}}{\overline{M}^{*(j)}_{\perp}} \tan\theta_E \quad (0 \leq \theta_j \leq 90^\circ)\,; \tag{5.36}$$

where the orientation angle,

$$\theta_E \stackrel{\text{def.}}{=} \tan^{-1}\frac{E_{\parallel}}{E_z}, \tag{5.37}$$

of the external field $\mathbf{E}$ is the same for all species. Equation (5.36) shows how the species-specific trajectory angle $\theta_j$ is determined by the respective components of the chromatographic mobility tensor for that species. An important parameter controlling these mobilities is the species-specific axial Peclet number,

$$\mathrm{Pe}^{(j)} \stackrel{\text{def.}}{=} \lambda_j \frac{E_z l_z}{kT}. \tag{5.38}$$

**Examples (Layered Fluid)** Three simple illustrations of the functional dependence of the chromatographic trajectory angle upon the several microscale parameters entering into its computation are presented below for the case of immiscible fluid layers. As the trajectory angle concept provides the key distinction existing between *vector* and *scalar* chromatography, we have deemed it significant to provide these illustrative examples, despite the artificiality of the layered-fluid model in the context of real micropatterned separation devices. Each example highlights the concept of vector chromatography in a different context, respectively emphasizing: (i) hydrodynamic and (ii) affinity vector chromatography, as well as (iii) providing an example of a vector separation that could not otherwise have been accomplished via traditional scalar chromatography.

*Hydrodynamic Vector Chromatography* ($\mu_1 \neq \mu_2$; $K^{(j)} = 1$)

Consider the separation of an ensemble of different species of Brownian spheres of, say, identical radii $a_j$ but with differing $\lambda_j$ values [see eq. (4.20)], where each solute species is assumed to form an ideal solution with both fluid layers. The animating field $\mathbf{E}$ is taken to be oriented at a field orientation angle of $\theta_E = 45°$. In such circumstances, the axial and transverse Peclet numbers are equal:

$$\mathrm{Pe}^{(j)} \longleftrightarrow \mathrm{Pe}_{\perp}^{(j)}. \tag{5.39}$$

Accordingly, only the axial Peclet number, $\mathrm{Pe}^{(j)}$, appears in subsequent calculations.

Application of eq. (5.36) yields, for the ideal solution case, $K^{(j)} = 1\ \forall j$,

$$\theta_j = \tan^{-1}\left\{1 + \left(2 - \frac{\mu_2}{\mu_1} - \frac{\mu_1}{\mu_2}\right)\frac{\left[1 - \exp(\mathrm{Pe}^{(j)}\,\epsilon_1)\right]\left[1 - \exp(\mathrm{Pe}^{(j)}\,\epsilon_2)\right]}{\mathrm{Pe}^{(j)}\left[1 - \exp(\mathrm{Pe}^{(j)})\right]}\right\}. \tag{5.40}$$

In such circumstances, for specified values of $\mu_1/\mu_2$ and $\epsilon_1$, the maximum possible trajectory angle, denoted by $\theta_0$, irrespective of species undergoing separation, arises in the dominant Brownian motion limit, $\mathrm{Pe} \rightarrow 0$:

$$\theta_0 = \tan^{-1}\left[\frac{(\mu_1\epsilon_1 + \mu_2\epsilon_2)\,(\mu_2\epsilon_1 + \mu_1\epsilon_2)}{\mu_1\mu_2}\right]. \tag{5.41}$$

This expression follows from passage to the $\mathrm{Pe} \rightarrow 0$ limit in eq. (5.40), as well as by substitution of the dominant Brownian motion effective viscosities (5.25) and (5.29) into (5.36). The corresponding minimum possible trajectory angle, $\theta_\infty = \tan^{-1} 1 = \theta_E$, arises in the weak Brownian motion limit, $\mathrm{Pe}^{(j)} \rightarrow \infty$, and is independent of the fluid viscosity as well as of the relative volumes occupied by the respective fluid layers, since the net particle motion occurs exclusively in the direction of the applied force. Since, according to (5.40), for a given $\lambda_j$ the separation is effected by the dependence of the solute trajectory upon the fluid viscosities, which is a purely hydrodynamic attribute, this chromatographic scheme might aptly be assigned the appellation "hydrodynamic vector chromatography."

Figure 5-3 shows the relative separation angle $\Delta\theta \stackrel{\text{def.}}{=} \theta_j - \theta_0$ that would exist between two species, one experiencing an interaction $\lambda_j$ and the other experiencing only a weak interaction

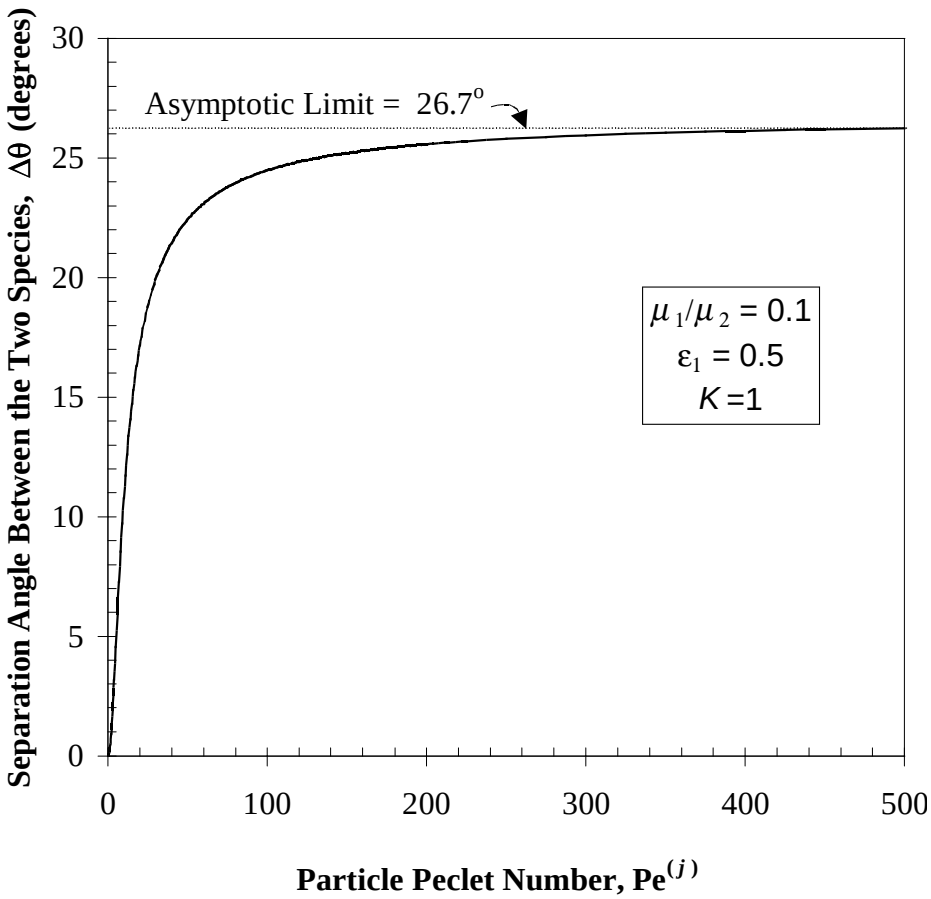


Figure 5-3: An example illustrating hydrodynamic vector chromatography: Relative separation angle $\Delta\theta_j \stackrel{\text{def.}}{=} \theta_j - \theta_0$ between a charged species $j$ characterized by a longitudinal particle Peclet number $\mathrm{Pe}^{(j)}$, and a weakly charged species ($\mathrm{Pe}^{(0)} \to 0$), for the fixed viscosity ratio and identical layered-phase volume fractions shown in the inset, and for the case of ideal solutions ($K = 1$).

force, $\lambda_0 \to 0$.[6] It is obvious from the data in Fig. 5-3 that separation of these two species could be effected quite readily were this layered device physically realizable, as the maximum separation angle, $\Delta\theta_{\max} \stackrel{\text{def.}}{=} \theta_\infty - \theta_0$, is over 26° for the prescribed parametric values.

*Affinity Vector Chromatography* ($K^{(j)} \neq 1$; $\mu_1 = \mu_2$)

It is readily verified that in the preceding example, where $K^{(j)} = 1$, that $\Delta\theta = 0\ \forall j$ in the homogeneous viscosity limit, $\mu_1 = \mu_2$, since it is precisely the microscale mobility inhomogeneity arising from the viscosity difference $|\mu_1 - \mu_2|$ that enables the separation to occur in the preceding thermodynamically ideal solution case. However, in the nonideal case, wherein $K^{(j)} \neq 1$, separation of species can be effected by exploiting physiochemical differences existing between the different solutes, even in circumstances where the viscosity inhomogeneity vanishes. Consider again the separation of an ensemble of Brownian spheres of identical radii $a_j$ animated by an externally applied field $\mathbf{E}$ oriented at a 45° angle with respect to the $z$-axis, but differing from the preceding example in that: (i) each particle experiences an identical $\lambda_j$ interaction with the field (whereby the index $j$ affixed to $\mathrm{Pe}^{(j)}$ may be suppressed); (ii) the viscosity ratio is $\mu_1/\mu_2 = 1$; and (iii) the several solute-solvent systems are non-ideal, with the extent of the non-ideality of each solute in the two different layers being embodied in the species-specific interphase partition coefficient,

$$K^{(j)} \stackrel{\text{def.}}{=} \frac{K_1^{(j)}}{K_2^{(j)}}. \tag{5.42}$$

Application of eq. (5.36) in these circumstances yields

$$\theta_j = \tan^{-1}\left\{1 - \frac{\left(K^{(j)} - 1\right)^2}{K^{(j)}} \frac{\left[1 - \exp(\mathrm{Pe}\,\epsilon_1)\right]\left[1 - \exp(\mathrm{Pe}\,\epsilon_2)\right]}{\mathrm{Pe}\left[1 - \exp(\mathrm{Pe})\right]}\right\}. \tag{5.43}$$

Physiochemical interactions between the solute and the solvent layers vanish in the ideal solution limit, $K^{(j)} = 1$, in which circumstance the particle trajectory lies along the direction of the field, whereupon the angle formed between the macroscopic velocity vector $\overline{\mathbf{U}}_j^*$ and the $z$-axis would be $\theta_0 = \theta_E = 45°$. However, when $K^{(j)} \neq 1$, eq. (5.43) shows the corresponding maximum

[6] While $\overline{\mathbf{U}}_0^* \to \mathbf{0}$ as $\lambda_0 \to 0$ (since $\mathbf{F}_0 \to \mathbf{0}$), the ratio $\overline{U}_\parallel^{*(0)} / \overline{U}_z^{*(0)}$ does not go to zero but, rather, tends to a definite limit, as then too does $\theta_0$.

angle to be $\theta_\infty = 90°$, occurring when the solute is essentially completely excluded from a given phase, say phase "2" in the case $K^{(j)} \to 0$. In such circumstances the mean particle trajectory would be entirely transverse to the viscosity gradient, parallel to the layers, despite the existence of a non-zero force component, $F_z$, attempting to cause the solute to translate across the layers.

Figure 5-4 presents the relative separation angle $\Delta\theta_j = \theta_j - \theta_0 \equiv \theta_j - 45°$ occurring between species $j$ for which $K^{(j)} \neq 1$, and another solute species, say "0", which forms ideal solutions with both phases ($K^{(0)} = 1$). Results shown include the dominant Brownian motion limiting case, Pe=0, as well as the case Pe=50, each for circumstances in which the composite medium consists of equal thicknesses of the immiscible fluid layers, possessing identical viscosities $\mu$. Separation is again readily effected in this situation, the separation being effected as a result of the existence of thermodynamic non-ideality forces, even in the dominant Brownian motion limit (equivalent to zero applied force). This dependence upon physiochemical interactions, involving the ability of the solute molecules to discriminate thermodynamically between the "continuous" and "discontinuous" phases, constitutes an example of what might be appropriately termed "affinity vector chromatography."

*Vector vs Scalar Chromatography*

While the spatio-temporal trajectory species separation provided by vector chromatography possesses the attractive feature of offering a *continuous* resolution scenario, one can envision circumstances for which the use of vector chromatography would prove *mandatory*, irrespective of this attribute, owing to the impossibility of effecting a classical scalar chromatographic separation between the species. Consider, for example, affinity chromatography ($K^{(j)} \neq 1$, $\mu_1$=$\mu_2$=$\mu$) for the immiscible layered-fluid geometry in the case of an ensemble of Brownian spheres of different radii possessing identical Peclet numbers (5.38), and whose radii are given fortuitously by the expression

$$a_j = a\frac{\mu}{\mu_\perp} \qquad (j = 1, 2, 3, \dots), \tag{5.44}$$

with $a$ is a characteristic radius (say, of the particle belonging to that species, say "0", forming ideal solutions with both layers, $K_0 = 1$). From the definition (5.44), it follows upon

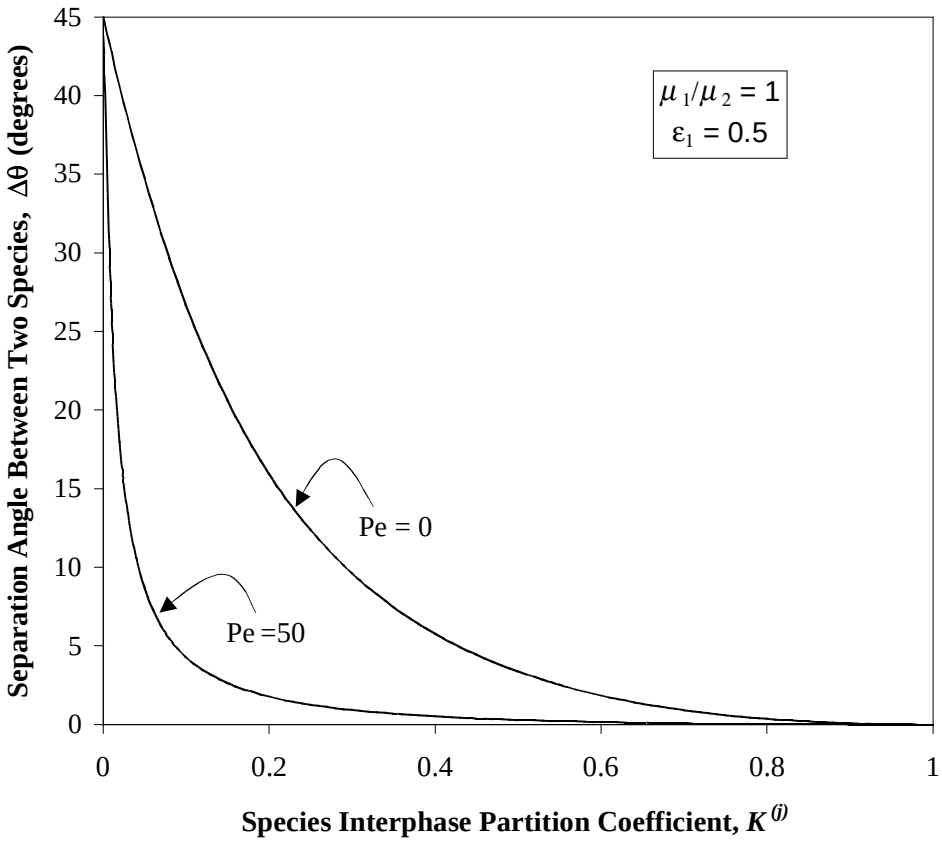


Figure 5-4: An example illustrating affinity vector chromatography: Relative separation angle $\Delta\theta_j \stackrel{\text{def.}}{=} \theta_j - \theta_0$ between a solute species $j$ forming a non-ideal solution ( $K^{(j)} \neq 1$) with the layered phases and an otherwise identical species that, however, forms an ideal solution with each of the layered phases ($K^{(0)} = 1$ ), for identical viscosities, identical layer volume fractions, and for several longitudinal Peclet numbers.

substitution of (5.23) into (1.1) that

$$\overline{U}_z^* = \frac{F_z}{6\pi\mu a}. \tag{5.45}$$

As this speed is independent of $j$, attempts to effect a separation of the various species possessing the indicated properties via scalar chromatography in the $z$-direction (i.e. collecting solute issuing from the bottom of the device at different times) would prove impossible since all of the solute species would exit the device, on average, at the same time. However, with the field $E$ oriented in a direction other than the $z$ direction, i.e. $\theta_E \neq 0$, application of (5.36) yields the trajectory angle

$$\tan\theta_j = \tan\theta_E \left\{ 1 + \frac{\left(K^{(j)} - 1\right)^2}{K^{(j)}} \frac{\left[1 - \exp(\mathrm{Pe}\,\epsilon_1)\right]\left[1 - \exp(\mathrm{Pe}\,\epsilon_2)\right]}{\mathrm{Pe}\left[1 - \exp(\mathrm{Pe})\right]} \right\}. \tag{5.46}$$

Accordingly, provided that the external field $\mathbf{E}$ was applied asymmetrically ($\tan\theta_E \neq 0$), the several solute species would exit the device, on average, at different locations, whence vector chromatographic separation would be achieved, despite the failure of scalar chromatography in such circumstances.

# Chapter 6

# Dispersivity

## 6.1 Continuous Periodic Viscosity Case

Subject to *a posteriori* verification, assume a trial function solution for the intracell $\mathbf{B}$ field of the form

$$\mathbf{B}(\mathbf{r}) = \mathbf{i}_z B_\perp(z) + \mathbf{i}_\| \mathrm{Pe}_\| B_\|(z) + (\mathbf{i}_z - \mathbf{r}), \tag{6.1}$$

where

$$\mathrm{Pe}_\| \stackrel{\text{def.}}{=} \frac{F_\| l_z}{kT} \tag{6.2}$$

is the transverse Peclet number. The form (6.1) is chosen such that the $z$-direction gradients in $P_0^\infty$ and viscosity appearing explicitly and implicitly in the governing equation (4.22) are incorporated into the trial functions $B_i(z)$ ($i = \|, \perp$), whereas the diminution (4.23), namely $-\|\mathbf{r}\|$, required in the $\mathbf{B}$ field in the transverse direction is accounted for by the linear combination $\mathbf{i}_z - \mathbf{r}$. The decrease in the $\mathbf{B}$ field in the $z$-direction is incorporated into the function $B_\perp$ [cf. eq. (6.5)]. Use of the transverse Peclet number (6.2) reduces the vector-valued partial differential equation (4.22) governing the vector $\mathbf{B}$ field to a pair of uncoupled scalar-valued ordinary differential equations in the axial and transverse directions respectively.

To simplify the notation, scale the trial functions with $l_z$ such that $B_i^*$ is the dimensionless

variable

$$B_i^* \stackrel{\text{def.}}{=} \frac{B_i}{l_z}, \quad (i = \perp, \|). \tag{6.3}$$

As was done earlier in connection with the dimensionless $z^*$ vs dimensional $z$ variables in (4.26), the asterisk affix in (6.3) will be suppressed throughout the subsequent analysis. Moreover, since knowledge only of $\nabla\mathbf{B}$, rather than of $\mathbf{B}$ itself, is needed to compute the dispersivity via (4.21), it is only necessary to calculate the gradients, $dB_i/dz$, of the trial functions appearing in (6.1), rather than the $B_i$'s themselves.

### 6.1.1 Calculation of $B_\perp$

Upon substituting into eq. (4.22) the chromatographic mobilities from (5.7)-(5.8) [in conjunction with use of (1.1)], the probability density $P_0^\infty$ from (5.4), and the flux density $\mathbf{J}_0^\infty$ calculated from (5.1) and (5.4), it is found that the second-order differential equation governing the $B_\perp$ field adopts the form

$$\frac{d}{dz}\left[\frac{P_0^\infty(z)}{\mu(z)}\frac{dB_\perp(z)}{dz}\right] - C\,\mathrm{Pe}\frac{dB_\perp(z)}{dz} = C\tau_0\mathrm{Pe}\,P_0^\infty(z) \qquad (0 < z < 1), \tag{6.4}$$

where, as in (5.6), $C$ is the constant of integration appearing in the expression for $P_0^\infty$. Equation (6.4) is to be solved subject to the following pair of jump boundary conditions:

$$B_\perp(1) - B_\perp(0) = -1, \tag{6.5}$$

$$\frac{dB_\perp(1)}{dz} - \frac{dB_\perp(0)}{dz} = 0. \tag{6.6}$$

To simplify the subsequent exposition of the solution scheme, define the function

$$\eta(z) \stackrel{\text{def.}}{=} \frac{\mu(z)}{\tau_0 P_0^\infty(z)}. \tag{6.7}$$

Integrating (6.4) twice and applying the above pair of jump boundary conditions eventually

yields

$$\frac{dB_\perp}{dz} = c_\perp \left[ 1 + C\tau_0 \,\mathrm{Pe}\, q^{-1}(z) \int_0^z dz' q(z')\eta(z') \right] + \tau_0^2 \, C \,\mathrm{Pe}\, \eta(z) \int_0^z dz' P_0^\infty(z') +$$
$$+ \tau_0^3 \, (C\,\mathrm{Pe})^2 \, \frac{\eta(z)}{q(z)} \int_0^z dz' q(z')\eta(z') \int_0^{z'} dz'' P_0^\infty(z''), \tag{6.8}$$

where $c_\perp$ is the constant of integration

$$c_\perp = -\eta(z) \frac{\tau_0^2 \, C \,\mathrm{Pe} \int_0^1 dz \, q(z)\eta(z) \int_0^z dz' P_0^\infty(z') + q(1)}{\int_0^1 dz \, q(z)\eta(z)}, \tag{6.9}$$

and $q(z)$ the integrating factor

$$q(z) = \exp\left( -C\tau_0 \,\mathrm{Pe} \int_0^z dz' \eta(z') \right). \tag{6.10}$$

Note that the second-order differential equation (6.4) produces only one non-arbitrary constant of integration, namely $c_\perp$, arising from the jump boundary condition (6.5). The second jump condition, eq. (6.6), redundantly reproduces the normalization condition set forth in eq. (4.19), which has already been satisfied. Hence, the second constant of integration may be arbitrarily set equal to zero without loss of generality.

### 6.1.2 Calculation of $B_\parallel$

The solution for the parallel case proceeds along similar lines. Explicitly, this field satisfies the differential equation

$$\frac{d}{dz} \left[ \frac{P_0^\infty(z)}{\mu(z)} \frac{dB_\parallel(z)}{dz} \right] = C \,\mathrm{Pe} \frac{dB_\parallel(z)}{dz} + P_0^\infty(z) \left[ 6\pi a \overline{M}_\parallel^* - \mu(z)^{-1} \right], \tag{6.11}$$

which is to be solved so as to satisfy the pair of jump boundary conditions

$$B_{\|}(1) - B_{\|}(0) = 0, \tag{6.12}$$

$$\frac{dB_{\|}(1)}{dz} - \frac{dB_{\|}(0)}{dz} = 0. \tag{6.13}$$

The sole differences existing between the respective transverse and axial differential equations (6.11) and (6.4) governing $B_{\|}$ and $B_{\perp}$ lie in the respective forcing functions appearing on the right-hand sides of these equations, and in the boundary conditions (6.12) vs (6.5). Hence, in the present case, a first integral similar to (6.14) is recovered, namely

$$\begin{aligned}\frac{dB_{\|}}{dz} =& c_{\|}\left[1 + C\,\tau_0\,\mathrm{Pe}\,q^{-1}(z)\int_0^z dz' q(z')\eta(z')\right] + \eta(z)\int_0^z dz'\zeta(z')dz' + \\ &+ C\,\tau_0\,\mathrm{Pe}\frac{\eta(z)}{q(z)}\int_0^z dz' q(z')\eta(z')\int_0^{z'} dz''\zeta(z''),\end{aligned} \tag{6.14}$$

with the same integrating factor $q(z)$ as in (6.10), but now with a constant of integration

$$c_{\|} = \frac{\eta(z)\displaystyle\int_0^1 dz\, q(z)\eta(z)\int_0^z dz'\zeta(z')}{\displaystyle\int_0^1 dz\, q(z)\eta(z)} \tag{6.15}$$

appearing in place of $c_{\perp}$. In the latter two expressions,

$$\zeta(z) = \tau_0 P_0^{\infty}(z)\left[6\pi a\overline{M}_{\|}^{*} - \mu(z)^{-1}\right]. \tag{6.16}$$

As in the previous axial case, only one nonarbitrary constant of integration arises from the solution of the second-order differential equation (6.11). In present circumstances, the boundary condition (6.13) redundantly reproduces the definition of the transverse macroscopic velocity component [obtained by substituting (5.26) into (1.1)], and hence does not constitute an independent condition to be satisfied. That the governing equation (4.22) and boundary conditions (4.23) have been satisfied by our trial function solution confirms *a posteriori* the

initially-assumed form (6.1) for $\mathbf{B}$.

### 6.1.3 Calculation of $\overline{\mathbf{D}}^*$

Upon substituting into (4.21) the microscale Stokes-Einstein equation (2.6b) together with (6.1), and noting that all functions appearing in the resulting integrand depend only upon $z$, one obtains

$$\overline{\mathbf{D}}^* = \mathbf{i}_z\mathbf{i}_z\overline{D}^*_{\perp\perp} + \left(\mathbf{i}_z\mathbf{i}_\parallel + \mathbf{i}_\parallel\mathbf{i}_z\right)\overline{D}^*_{\parallel\perp} + (\mathbf{I} - \mathbf{i}_z\mathbf{i}_z)\overline{D}^*_{\parallel\parallel}, \tag{6.17}$$

wherein

$$\overline{D}^*_{\perp\perp} = \frac{kT}{6\pi a}\int_0^1 dz\,\eta^{-1}(z)\left[\mathrm{Pe}_\parallel^2\left(\frac{dB_\parallel}{dz}\right)^2 + \left(\frac{dB_\perp}{dz}\right)^2\right], \tag{6.18a}$$

$$\overline{D}^*_{\parallel\perp} \equiv \overline{D}^*_{\perp\parallel} = -\frac{kT}{6\pi a}\mathrm{Pe}_\parallel\int_0^1 dz\,\eta^{-1}(z)\frac{dB_\parallel}{dz}, \tag{6.18b}$$

$$\overline{D}^*_{\parallel\parallel} = \frac{kT}{6\pi a}\int_0^1 dz\,\eta^{-1}(z) \equiv kT\overline{M}^*_\parallel. \tag{6.18c}$$

The last equality follows from the first of equations (5.8). Owing to the fact that $\overline{\mathbf{D}}^*$ is a positive-definite dyadic [12], the three scalar dispersion coefficients appearing in (6.1.3) necessarily obey the trio of inequalities

$$\overline{D}^*_{\perp\perp} > 0, \quad \overline{D}^*_{\parallel\parallel} > 0, \quad \overline{D}^*_{\perp\perp}\overline{D}^*_{\parallel\parallel} > \left(\overline{D}^*_{\parallel\perp}\right)^2 \tag{6.19}$$

since the eigenvalues of the symmetric dyadic $\overline{\mathbf{D}}^*$ are positive.[1]

In general, no counterpart of $\overline{D}^*_{\parallel\parallel}$ will exist in micropatterned devices etched onto chips (except for the "molecular" dispersivity in the $\mathbf{I} - \mathbf{i}_z\mathbf{i}_z$ direction, which would be incorporated into the $\overline{D}^*_{\parallel\perp}$ component in the latter devices). This third component appears in our analysis only because our spatially periodic geometry extends into the third dimension. As such, only

[1] Although it may appear physically counter-intuitive that $\overline{D}^*_{\parallel\perp}$ is negative, as is subsequently shown to be the case, the positive eigenvalues of $\overline{\mathbf{D}}^*$ ensure satisfaction of the physical requirement that the dispersivity components be positive along their principal directions of $\overline{\mathbf{D}}^*$.

two components of the dispersivity tensor are to be expected in applications to etched periodic structures, reflecting the latter's two-dimensional lattice configuration.

Although the complex forms of the integrands (6.18a) and (6.18b) preclude the possibility of effecting their integrations in closed form, several important features (besides obvious symmetry aspects) can readily be extracted from these expressions. Whereas the principal axes of the *microscale* mobility and diffusivity (dispersivity) tensors are colinear as a result of the Stokes-Einstein equation $\mathbf{D} = kT\mathbf{M}$, no comparable relationship exists between their macroscale counterparts, $\overline{\mathbf{D}}^*$ and $\overline{\mathbf{M}}^*$. Accordingly, the Nernst-Planck-Einstein equation will generally not apply at the macroscale, except under highly restrictive circumstances.[2] This generally negative conclusion accords with the theoretical work of Slater *et al.* [23], as well as with the experimental gel electrophoresis work of Gibson & Sepaniak [24]. Their studies observed that macroscale mobility and dispersivity are not related by the Nernst-Planck-Einstein equation for two-dimensional reptation of DNA through electrophoretic gels, nor for theoretical models thereof. This lack of correlation among these two parameters does not stem exclusively from the micromechanics of the solute motion, i.e. reptation [25]. Rather, it arises as a consequence of the force-driven flux contribution (above and beyond the diffusive flux) to the overall solute dispersion process, quantified by the respective magnitudes of the several Peclet numbers. Moreover, this negation of the macroscale Nernst-Plank-Einstein equation is further reinforced by the fact that a non-zero dispersivity component $\overline{D}^*_{\parallel\perp}$ (6.18b) exists without there being a comparable component, $\overline{M}^*_{\parallel\perp}$, of the chromatographic mobility dyadic (5.7).

As a final comment on the general form of the dispersivity, in the elementary sinusoidal viscosity variation case (5.9) we were unable to effect a closed-form quadrature of the requisite dispersivity integral (4.21), despite having in our possession a closed-form expression for the integrand appearing therein. As was also true of the comparable mobility calculation, this fact serves to underscore the future analytical difficulties anticipated when computing dispersion coefficients in geometrically, physiochemically, and hydrodynamically more realistic micropatterned systems than those under discussion in our illustrative, variable viscosity examples. Rather, progression to more realistic systems, such as microlithographic arrays, will inevitably

[2] As an example of the restrictive circumstances necessary for its macroscale validity, the Nernst-Plank-Einstein equation will subsequently be shown to hold in the force-free, pure hindered molecular diffusion limit [cf. §6.3].

involve extensive numerical computations, in which the unit cell $P_0^\infty$ and $\mathbf{B}$ fields required in the generic formulas (4.12) and (4.21) for determining $\overline{\mathbf{U}}^*$ and $\overline{\mathbf{D}}^*$ can only be obtained numerically, as opposed to our having obtained them analytically in the present elementary examples.

## 6.2 Immiscible Layered-Fluid Case

Subject to *a posteriori* verification, assume the following piecewise continuous $\mathbf{B}$ field, similar to the trial function solution (6.1) used in the previous continuous viscosity case:

$$\mathbf{B}(\mathbf{r}) = \begin{cases} \mathbf{B}_1 & (0 < z < \epsilon_1)\,, \\ \mathbf{B}_2 & (\epsilon_1 < z < 1)\,, \end{cases} \tag{6.20}$$

wherein

$$\mathbf{B}_i = \mathbf{i}_z B_{\perp,i}(z) + \mathbf{i}_\perp \mathrm{Pe}_\| B_{\|,i}(z) + (\mathbf{i}_z - \mathbf{r}) \;\; (i = 1, 2)\,. \tag{6.21}$$

The governing equations for the $B_\perp$ and $B_\|$ fields appearing in the preceding are respectively identical to eqs. (6.4) and (6.11), and apply separately within each of the two phases, provided that: (i) the viscosities are defined by (5.13); (ii) the constant $C$ is replaced with $\hat{C}$, as in (5.18); and (iii) $\overline{M}_\|^*$ for the immiscible layered fluid is given by (5.26). To the jump boundary conditions in (6.5)-(6.6) and (6.12)-(6.13) must now be added the additional constraints: (i) that $B_\perp$ and $B_\|$ are each continuous across the interface $z = \epsilon_1$, as required by eq. (4.24); and (ii) the generic flux continuity relationship of (4.25) must be satisfied, requiring that

$$\frac{K_2}{\mu_1}\frac{dB_{i,1}}{dz} = \frac{K_1}{\mu_2}\frac{dB_{i,2}}{dz} \quad \text{at} \quad z = \epsilon_1 \quad (i = \perp, \|). \tag{6.22}$$

### 6.2.1 Calculation of $B_\perp$

Solution of the governing equation in the perpendicular direction, subject to the stated jump and interface boundary conditions, requires that[3]

$$\frac{dB_{\perp,1}}{dz} = \frac{c_{\perp,1}}{q_{\perp,1}(z)} + \frac{\mu_1}{\mu_\perp}\mathrm{Pe}\int_0^z dz' q_{\perp,1}(z'),$$
$$\frac{dB_{\perp,2}}{dz} = \frac{c_{\perp,2}}{q_{\perp,2}(z)} + \frac{\mu_2}{\mu_\perp}\mathrm{Pe}\int_{\epsilon_1}^z dz' q_{\perp,2}(z'), \tag{6.23}$$

with integrating functions

$$q_{\perp,1}(z) = \frac{P^\infty_{0(1)}(z)}{P^\infty_{0(1)}(0)}\exp\left(-\frac{\mathrm{Pe}}{\tau_0}\frac{\mu_1}{\mu_\perp}\int_0^z \frac{dz'}{P^\infty_{0(1)}(z')}\right),$$
$$q_{\perp,2}(z) = \frac{P^\infty_{0(2)}(z)}{P^\infty_{0(2)}(\epsilon_1)}\exp\left(-\frac{\mathrm{Pe}}{\tau_0}\frac{\mu_2}{\mu_\perp}\int_{\epsilon_1}^z \frac{dz'}{P^\infty_{0(2)}(z')}\right), \tag{6.24}$$

and integration constants

$$c_{\perp,1} = -\frac{\mathrm{Pe}\left[\frac{\mu_1}{\mu_\perp}\int_0^{\epsilon_1} dz \int_0^z dz' q_{\perp,1}(z') + \frac{\mu_2}{\mu_\perp}\int_{\epsilon_1}^1 dz \int_{\epsilon_1}^z dz' q_{\perp,2}(z') + \frac{K_2\mu_2}{K_1\mu_\perp}\int_0^{\epsilon_1} dz\, q_{\perp,1}(z)\int_{\epsilon_1}^1 \frac{dz}{q_{\perp,2}(z)}\right] + 1}{\int_0^{\epsilon_1}\frac{dz}{q_{\perp,1}(z)} + \frac{K_2\,\mu_2}{K_1\mu_1}\frac{1}{q_{\perp,1}(\epsilon_1)}\int_{\epsilon_1}^1 \frac{dz}{q_{\perp,2}(z)}},$$
$$c_{\perp,2} = \frac{K_2\mu_2}{K_1\mu_1}\left(\frac{c_{\perp,1}}{q_{\perp,1}(\epsilon_1)} + \mathrm{Pe}\frac{\mu_1}{\mu_\perp}\int_0^{\epsilon_1} dz\, q_{\perp,1}(z)\right). \tag{6.25}$$

The respective forms of the gradients (6.23) and integration constants (6.25) differ from those for the continuous viscosity case [cf. eqs. (6.8)-(6.10)] as a consequence of our solution scheme. In the continuous viscosity case it was convenient to initially integrate the entire equation and

[3]Similar to the $P_0^\infty$ field, the derivatives in (6.23) appear superficially not to satisfy the requisite jump boundary condition $\|\nabla\mathbf{B}\| = \mathbf{0}$ on $\partial\tau_0$. As before, this apparent inconsistency can be remedied without, of course, altering the ultimate form for $\overline{\mathbf{D}}^*$ by adjusting the arbitrary choice of location for the unit cell faces relative to the interface, such that neither of the two $z$-face cell boundaries coincides with the phase interface $s_p$. This will also be true for $B_\parallel$ [cf. (6.26)].

subsequently solve the resulting first-order ordinary differential equation. However, for the present immiscible layered-fluid case the constant viscosities rendered it simpler to reverse the order of these two steps, so as to initially solve a first-order differential equation for $dB_{\perp,i}/dz$, subsequent to integration.

### 6.2.2 Calculation of $B_{\parallel}$

Proceeding to the comparable parallel trial function calculations, the gradients within each phase are found to possess the respective forms

$$\frac{dB_{\parallel,1}}{dz} = \left(\frac{\mu_1}{\mu_\parallel} - 1\right) \frac{c_{\parallel,1} + \int\limits_0^z dz' q_{\parallel,1}(z')}{q_{\parallel,1}(z)},$$
$$\frac{dB_{\parallel,2}}{dz} = \left(\frac{\mu_2}{\mu_\parallel} - 1\right) \frac{c_{\parallel,2} + \int\limits_{\epsilon_1}^z dz' q_{\parallel,2}(z')}{q_{\parallel,2}(z)}, \tag{6.26}$$

with integrating factors

$$q_{\parallel,1}(z) = \frac{P^{\infty}_{0(1)}(z)}{P^{\infty}_{0(1)}(0)} \exp\left(-\frac{\mathrm{Pe}}{\tau_0}\frac{\mu_1}{\mu_\parallel}\int\limits_0^z \frac{dz'}{P^{\infty}_{0(1)}(z')}\right),$$
$$q_{\parallel,2}(z) = \frac{P^{\infty}_{0(2)}(z)}{P^{\infty}_{0(2)}(\epsilon_1)} \exp\left(-\frac{\mathrm{Pe}}{\tau_0}\frac{\mu_2}{\mu_\parallel}\int\limits_{\epsilon_1}^z \frac{dz'}{P^{\infty}_{0(2)}(z')}\right), \tag{6.27}$$

and integration constants

$$c_{\|,1} = \frac{\left[\begin{array}{c} \left(1-\frac{\mu_1}{\mu_\|}\right)\int\limits_0^{\epsilon_1} dz\, q_{\|,1}^{-1}(z)\int\limits_0^{z} dz' q_{\|,1}(z') + \left(1-\frac{\mu_2}{\mu_\|}\right)\int\limits_{\epsilon_1}^{1} dz\, q_{\|,2}^{-1}(z)\int\limits_{\epsilon_1}^{z} dz' q_{\|,2}(z') - \\ -\frac{K_2\mu_2}{K_1\mu_1}\left(1-\frac{\mu_1}{\mu_\|}\right) q_{\|,1}^{-1}(\epsilon_1)\int\limits_0^{\epsilon_1} dz\, q_{\|,1}(z)\int\limits_{\epsilon_1}^{1}\frac{dz}{q_{\|,2}(z)} \end{array}\right]}{\int\limits_0^{\epsilon_1}\frac{dz}{q_{\|,1}(z)} + \frac{K_2\mu_2}{K_1\mu_1}\frac{1}{q_{\|,1}(\epsilon_1)}\int\limits_{\epsilon_1}^{1}\frac{dz}{q_{\|,2}(z)}},$$

$$c_{\|,2} = \frac{K_2\mu_2}{K_1\mu_1} q_{\|,1}^{-1}(\epsilon_1)\left[c_{\|,1} + \left(\frac{\mu_1}{\mu_\|}-1\right)\int\limits_0^{\epsilon_1} dz\, q_{\|,1}(z)\right]. \tag{6.28}$$

That the governing equation (4.22) and jump boundary conditions (4.23) have all been satisfied serves to verify *a posteriori* the trial function form (6.20) initially assumed for $\mathbf{B}$.

### 6.2.3 Calculation of $\overline{\mathbf{D}}^*$

Having now calculated $\nabla\mathbf{B}$, the dispersivity components may be computed from eq. (6.1.3) via piecewise integration. Explicitly, the dispersivity components are thereby obtained

$$\overline{D}^*_{\perp\perp} = \frac{kT}{6\pi a}\tau_0\left\{\begin{array}{c} \int\limits_0^{\epsilon_1} dz \frac{P^\infty_{0(1)}(z)}{\mu_1}\left[\mathrm{Pe}_\|^2\left(\frac{dB_{\|,1}}{dz}\right)^2 + \left(\frac{dB_{\perp,1}}{dz}\right)^2\right] + \\ + \int\limits_{\epsilon_1}^{1} dz\, \frac{P^\infty_{0(2)}(z)}{\mu_2}\left[\mathrm{Pe}_\|^2\left(\frac{dB_{\|,2}}{dz}\right)^2 + \left(\frac{dB_{\perp,2}}{dz}\right)^2\right] \end{array}\right\}, \tag{6.29a}$$

$$\overline{D}^*_{\|\perp} = -\frac{kT}{6\pi a}\tau_0\,\mathrm{Pe}_\|\left[\int\limits_0^{\epsilon_1} dz\,\frac{P^\infty_{0(1)}(z)}{\mu_1}\frac{dB_{\|,1}}{dz} + \int\limits_{\epsilon_1}^{1} dz\,\frac{P^\infty_{0(2)}(z)}{\mu_2}\frac{dB_{\|,2}}{dz}\right], \tag{6.29b}$$

$$\overline{D}^*_{\|\|} = kT\overline{M}^*_\|. \tag{6.29c}$$

Whereas the integrating functions $q_i(z)$ appearing in the above expressions for $dB_i/dz$ ($i = \|, \perp$) possess closed forms, no comparable closure exists for the integral of $q_i(z)$ itself. As such, numerical integration is necessary to determine the dispersivity for each prescribed set of microscale data. Despite our having to resort to such numerics, the general remarks offered in connection with the dispersivity for the continuous viscosity case apply equally well here, namely

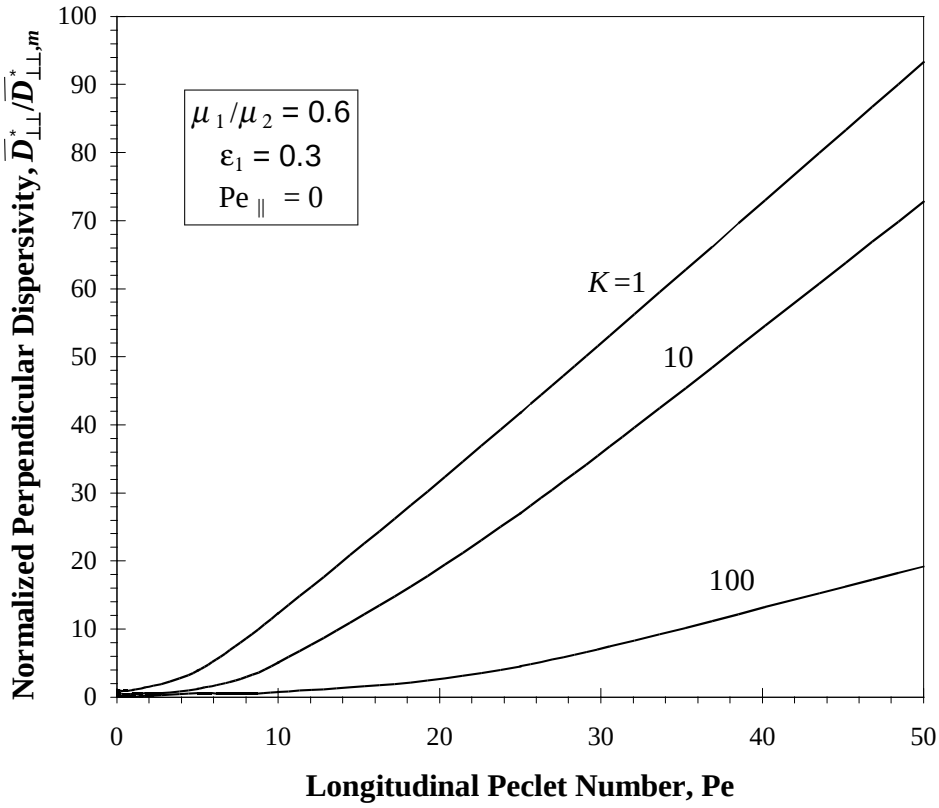


Figure 6-1: Dependence of the $\overline{D}^*_{\perp\perp}$ component of the layered-fluid dispersivity tensor [normalized with the zero-force, equi-partitioned ($K$=1), hindered molecular dispersivity component $\overline{D}^*_{\perp\perp,m}$] upon the longitudinal Peclet number Pe for several thermodynamic partition coefficient values and for the prescribed values of the other parameters shown in the inset.

that the dispersivity dyadic is symmetric, and that a Nernst-Planck-Einstein-type equation generally fails to exist.

Figure 6-1 presents results obtained numerically for the $\overline{D}^*_{\perp\perp}$ component (6.29a) of the dispersivity tensor, normalized using the dispersivity obtained for the equally-partitioned perpendicular case [cf. (6.33) with $K_1 = K_2$]. The impact of the force upon the dispersivity component is apparent, since each curve grows exponentially with increasing Pe. Increasing the extent of non-ideality of a given phase, as quantitatively embodied in the partition coefficient $K$, decreases the overall dispersivity, since deviations of the particle from its mean trajectory becomes increasingly difficult as $K$ tends towards infinity owing to the fact that the particle

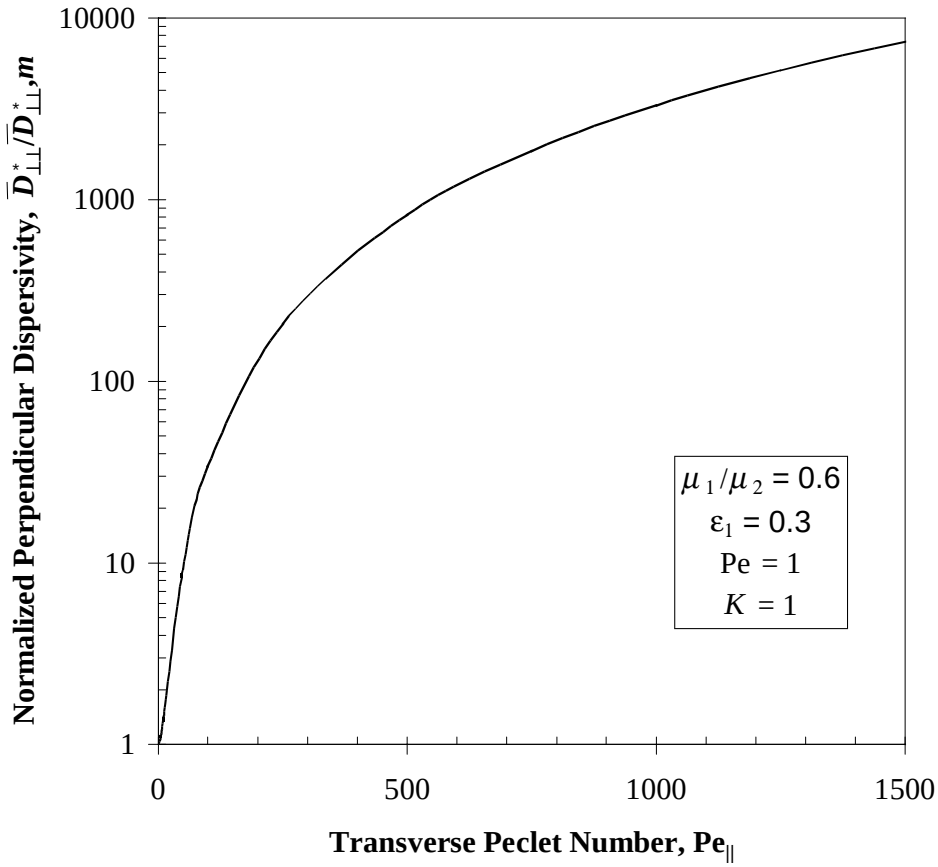


Figure 6-2: Dependence of the $\overline{D}^*_{\perp\perp}$ component of the layered dispersivity tensor [normalized with the zero-force, equi-partitioned ($K$=1), hindered molecular dispersivity component $\overline{D}^*_{\perp\perp,m}$ ] upon the transverse Peclet number $Pe_{\|}$, and for the fixed parametric values shown in the inset.

spends the majority of its time in only one of the two phases.[4] These two trends serve to further illustrate the absence of a Nernst–Planck-Einstein relationship at the macroscale. Convective effects arising from the action of external forces, physically lacking in the underlying derivation of the classical molecular Stokes-Einstein equation [26], contribute to the macroscopic dispersivity in the present physical situation, and hence account for the lack of a comparable relationship (in this particular case, between $\overline{D}^*_{\perp\perp}$ and $\overline{M}^*_{\perp}$).

[4]The lack of dependence of $\overline{D}^*_{\perp\perp}$ upon the arbitrary choice of phase labels and origin reveals that Fig. 6-1 also corresponds to circumstances where $\mu_1/\mu_2 = 5/3$ and $\epsilon_1 = 0.7$ for the values $K$=1, 0.1, and 0.01. Accordingly, the dispersivity is maximized at $K = 1$ since solute motion in that limit is unimpeded by thermodynamic forces.

Figure 6-2 presents dispersivity data similar to that given in Fig. 6-1, except that now the results are presented as a function of the transverse Peclet number $\mathrm{Pe}_{\parallel}$ for the case where the longitudinal Peclet number Pe=1. The inclusion of forces parallel to the layers causes this dispersivity component to grow exponentially with $\mathrm{Pe}_{\parallel}$, rather than quadratically, as might otherwise have been expected from a cursory examination of (6.29a). In fact, the transverse Peclet number serves to quadratically augment the exponential effect of the longitudinal Peclet number, which is itself implicitly embodied in the functions $dB_{\parallel,1}/dz$ and $dB_{\parallel,2}/dz$ appearing in the integrand of (6.29a). Moreover, this observation reinforces our prior remarks regarding the impact of transverse forces upon the overall dispersivity.

The general inapplicability of a macroscale Nernst-Planck-Einstein equation is again readily confirmed by Fig. 9, which presents the numerical results obtained for $-\overline{D}^*_{\parallel\perp}$, normalized as before.[5] Figure 9 displays the linear dependence of $-\overline{D}^*_{\parallel\perp}$ upon the transverse Peclet number, a fact readily apparent from eq. (6.29b). Since non-zero values of $\overline{D}^*_{\parallel\perp}$ are achieved for any non-zero value of $\mathrm{Pe}_{\parallel}$, it is obvious that $\overline{\mathbf{D}}^* \neq kT\overline{\mathbf{M}}^*$ in these circumstances. The latter negation is further strengthened by the fact that this "mixed" dispersivity component continues to increase with $\mathrm{Pe}_{\parallel}$, albeit much more slowly than does the $\overline{D}^*_{\perp\perp}$ component in comparable circumstances.

## 6.3 Immiscible Layered-Fluid Case (Dominant Brownian Motion)

In the dominant Brownian motion, effective zero-force limit, Pe$\rightarrow 0$, the dispersivity reduces to a simple closed-form expression, one which may be interpreted as a hindered molecular dispersivity, such hindrance arising from the "tortuous" path followed by a Brownian solute molecule traversing the periodic system, while wending its way around the obstacles. The convective contribution to the dispersivity vanishes in this limit, thereby reducing the dispersivity to but

[5] The continued choice of the normalization factor $D^*_{\perp\perp,m}$, used to render the results dimensionless, is entirely arbitrary since the dominant Brownian motion, hindered molecular dispersivity component, $D^*_{\parallel\perp,m}$, vanishes identically.

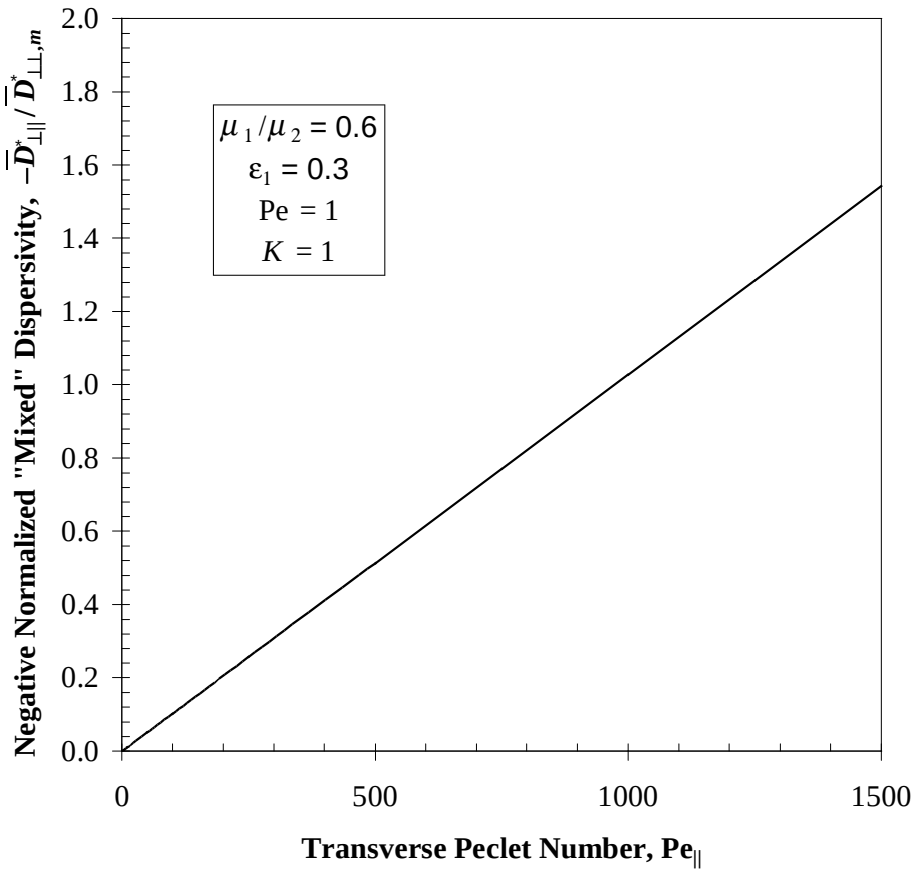


Figure 6-3: Dependence of the $-\overline{D}^*_{\perp\parallel}$ component of the layered dispersivity tensor [normalized with the zero-force, equi-partitioned ($K$=1), hindered molecular parallel dispersivity component $\overline{D}^*_{\perp\perp,m}$] upon the transverse Peclet number $\mathrm{Pe}_{\parallel}$ for the prescribed values of the other parameters shown in the inset.

two independent components:

$$\overline{\mathbf{D}}^* = \mathbf{i}_z\mathbf{i}_z\overline{D}^*_{\perp\perp,m} + (\mathbf{I} - \mathbf{i}_z\mathbf{i}_z)\,\overline{D}^*_{\parallel\parallel,m}, \tag{6.30}$$

where the subscript $m$ is appended to indicate that the dispersivity arises due solely to molecular effects, albeit hindered. The mixed component $\overline{D}^*_{\parallel\perp}$ is necessarily zero since it depends linearly on the transverse force $F_\parallel$, which is zero in present circumstances.

### 6.3.1 Calculation of $\overline{D}^*_{\perp\perp,m}$

Since, from (5.21), the probability density within each phase is independent of position, and since the Peclet number terms vanish in the present case, the piecewise gradients of the perpendicular trial function adopt the respective forms

$$\frac{dB_\perp}{dz} = \begin{cases} -\dfrac{K_1\mu_1}{K_1\mu_1\epsilon_1 + K_2\mu_2\epsilon_2} & (0 < z < \epsilon_1)\,, \\ -\dfrac{K_2\mu_2}{K_1\mu_1\epsilon_1 + K_2\mu_2\epsilon_2} & (\epsilon_1 < z < 1)\,. \end{cases} \tag{6.31}$$

Upon performing the requisite integrations and subsequent algebraic manipulations, one obtains

$$\overline{D}^*_{\perp\perp,m} = \frac{K_1K_2kT}{6\pi a\,(K_1\mu_1\epsilon_1 + K_2\mu_2\epsilon_2)\,(K_2\epsilon_1 + K_1\epsilon_2)}. \tag{6.32}$$

Equivalently, by using the fact that $D_i = kT\,(6\pi a\mu_i)^{-1}$ $(i = 1, 2)$, the above may be rewritten alternatively as

$$\frac{1}{\overline{D}^*_{\perp\perp,m}} = \frac{(K_2\epsilon_1 + K_1\epsilon_2)}{K_1K_2}\left(\frac{K_1\epsilon_1}{D_1} + \frac{K_2\epsilon_2}{D_2}\right). \tag{6.33}$$

In the limit, $K_1 = K_2$, of equal partitioning, $\overline{D}^*_{\perp\perp,m}$ may be regarded as arising from resistances in series.

### 6.3.2 Calculation of $\overline{D}^*_{\parallel\parallel,m}$

Substitution of the Pe=0 solutions (5.21)-(5.22) for $P_0^\infty$ into the integrand of (6.18c) yields

$$\overline{D}^*_{\parallel\parallel,m} = \frac{kT}{6\pi a\left(K_2\epsilon_1 + K_1\epsilon_2\right)}\left(\frac{K_2\epsilon_1}{\mu_1} + \frac{K_1\epsilon_2}{\mu_2}\right). \tag{6.34}$$

The latter may be written alternatively in terms of the molecular diffusivity via the microscale Stokes-Einstein equation (2.6b), to obtain

$$\overline{D}^*_{\parallel\parallel,m} = \frac{K_2\epsilon_1 D_1 + K_1\epsilon_2 D_2}{K_2\epsilon_1 + K_1\epsilon_2}. \tag{6.35}$$

As in the corresponding mobility case, irrespective of the extent of partitioning, the above may be qualitatively interpreted as manifesting the phenomenon of resistances in parallel when the viscosity $\mu_j$ appearing in the mobility expression $M_j = (6\pi a\mu_j)^{-1}$ $(j = 1, 2)$ is interpreted as constituting a resistance in the Stokes-Einstein equation, $D_j = kTM_j$. In the limit $K_1 = K_2$ of equal partitioning, eq. (6.35) corresponds exactly to resistances in parallel.

The results obtained for $\overline{D}^*_{\perp\perp,m}$ and $\overline{D}^*_{\parallel\parallel,m}$accord with those of Brenner & Edwards [12], who considered the case of pure molecular diffusion through periodically layered, two-element media, each possessing different molecular diffusivities. As a final note, observe that it is only in the zero-force limit that the macroscale Stokes-Einstein relationship is valid.

# Chapter 7

# Concluding Remarks

The relative simplicity of the preceding steady-state microtransport calculations within a single unit cell employed to calculate the macroscale phenomenological coefficients $\overline{\mathbf{M}}^*$ and $\overline{\mathbf{D}}^*$, in comparison with the intractability of attempting to extract these coefficients via eqs. (4.4)-(4.5) and (4.7)-(4.8), respectively, from the solution of the underlying unsteady-state, initial- and boundary-value microtransport problem posed, demonstrates the overwhelming advantages of the former scheme in elucidating gross chromatographic behavior in spatially periodic systems, such as arises in micropatterned devices. Within the macrotransport paradigm [12], analytic expressions were developed for the dependence of the chromatographic mobility and dispersivity dyadics $\overline{\mathbf{M}}^*$ and $\overline{\mathbf{D}}^*$ upon: (i) the respective longitudinal and transverse Peclet numbers, Pe and $\mathrm{Pe}_{\|}$; (ii) the interphase thermodynamic solute partition coefficient $K = K_1/K_2$; (iii) the periodic viscosity field $\mu(z)$; and (iv) the geometrical factors characterizing the spatial periodicity. Moreover, the two simple examples considered, namely the continuous and discontinuous periodic viscosity cases, definitively demonstrated the resulting anisotropy of the chromatographic mobility, an attribute which will necessarily obtain in all asymmetric[1] spatially periodic micropatterned devices — thereby giving rise to the concept of "vector chromatography."

One cannot help but be struck by the algebraic complexity and distinctly counter-intuitive nature of many of our final results, even for the two elementary physical geometric configurations

[1]By "asymmetric" is meant that the point-group symmetry of the microscale obstacle geometry is not isotropic with regard to second-rank tensors, as discussed in Note 6. In such asymmetric circumstances, $\overline{\mathbf{U}}^*$ will not generally lie parallel to $\mathbf{F}$ unless, perchance, the orientation of this space-fixed vector $\mathbf{F}$ lies parallel to one of the body-fixed eigenvectors of the symmetric chromatographic mobility dyadic $\overline{\mathbf{M}}^*$.

examined in this paper. As an explicit example of this counter-intuitive behavior, consider the layered-fluid case for circumstances wherein the vector force $\mathbf{F}$ (say, gravitational in origin, with the two fluids possessing the same densities so that $\mathbf{F} = \mathbf{i}_z F$ is independent of $z$) is oriented in the $z$-direction, so that the Brownian sphere translates, on average, only in that direction — alternately through layers "1" and "2". In the two individually homogeneous layers, considered separately, the solute particle will traverse the layers at the respective mean velocities

$$\overline{U}_1^* = \frac{F_z}{6\pi\mu_1 a}, \quad \overline{U}_2^* = \frac{F_z}{6\pi\mu_2 a}, \tag{7.1}$$

since the existence of the Brownian motion has no *net* effect upon the Stokes-law sedimentation velocity within a given homogeneous phase. The mean intraphase transit times, $t_1$ and $t_2$, required for the sphere to negotiate the respective layers of lengths $l_1 = \epsilon_1 l_z$ and $l_2 = \epsilon_2 l_z$ at these velocities would then be

$$t_1 = \frac{l_1}{\overline{U}_1^*}, \quad t_2 = \frac{l_2}{\overline{U}_2^*}. \tag{7.2}$$

As such, the mean time, $t$, say, required for the Brownian sphere to traverse one period (of total length $l_z$, corresponding to a unit cell) would be

$$t = t_1 + t_2, \tag{7.3}$$

and the distance covered in this time would be

$$l_z = l_1 + l_2. \tag{7.4}$$

Accordingly, intuition suggests a mean settling time for this composite layered series configuration as

$$\overline{U}_z^* = \frac{\text{distance}}{\text{time}} = \frac{l_1 + l_2}{t_1 + t_2}, \tag{7.5}$$

giving rise to an expected macroscale axial mobility, $\overline{M}^*_\perp \stackrel{\text{def.}}{=} \overline{U}^*_z/F_z$, of the form

$$\overline{M}^*_\perp \stackrel{?}{=} \frac{1}{6\pi a\,(\epsilon_1\mu_1 + \epsilon_2\mu_2)}, \tag{7.6}$$

independently of the Brownian motion. Equation (7.6) is, in fact, incorrect since it predicts that the mobility $\overline{M}^*_\perp$ is independent of the (longitudinal) Peclet number Pe$=F_z l_z/kT$, and hence of the magnitude $F_z$ of the force giving rise to the motion! This intuitive expectation stands in sharp contrast to the correct result, given in eqs. (5.23)-(5.24). What is counter-intuitive here is that, whereas Brownian motion effects on net particle motion within each phase taken separately are irrelevant, they are nevertheless sensible *en toto*. Moreover, the fact that the purely physiochemical (thermodynamic) partition coefficient $K$ plays a role in the correct calculation, (5.23)-(5.24), is also counter-intuitive since, from the point of view of either the hydrodynamics or the Brownian motion, the "surface properties" of the Brownian sphere — which presumably control the magnitude of the solute contribution to the degree of solute-solvent non-ideality — would not have been expected to affect the mean sedimentation velocity.[2] Such physiochemical surface properties are irrelevant when the sphere moves through a single, homogeneous fluid.[3]

The source of the non-zero Brownian motion contribution to the mobility in the present heterogeneous viscosity case, compared with the lack of a corresponding contribution in the homogeneous viscosity case with equal partitioning (such that no spatially periodic homogeneity remains within the system), can be traced to the fundamental disparity existing between the formula (4.12)-(4.13) furnishing $\overline{\mathbf{U}}^*$ for the spatially periodic viscosity case, and the comparable "unidirectional" (chromatographic) velocity formula [12],

$$\overline{\mathbf{U}}^* = \int_{\mathbf{q}_0} d\mathbf{q}\, P_0^\infty(\mathbf{q})\mathbf{M}(\mathbf{q})\cdot\mathbf{F}, \tag{7.7}$$

[2]On the other hand, one would certainly have expected the Brownian motion to affect the dispersivity $\overline{D}^*_{\perp\perp}$ for this case because of the differences existing in the sedimentation velocities of the sphere in the respective phases, giving rise to a $z$-dependent velocity deviation, $\mathbf{U}_i(z) - \overline{\mathbf{U}}^*$, within phase $i$ ($i = 1, 2$) from the composite mean velocity $\overline{\mathbf{U}}^*$.

[3]For example, it is well known that the no-slip boundary condition at the interface between a solid and liquid holds independently of whether or not the surface of the solid is "wetted" by the liquid (albeit a conclusion perhaps limited to physiochemically homogeneous surfaces in order to avoid Marangoni forces [15]).

that would prevail in its stead for the case of a *nonperiodic* system whose motion is animated by the external force $\mathbf{F}$. In eq. (7.7), $\mathbf{q}$ represents the so-called "local-space" variable in generic macrotransport theory notation, and $\mathbf{q}_0$ the local-space integration domain [12]. The difference between eqs. (4.12)-(4.13) and (7.7) lies in the presence of a direct Brownian motion contribution, namely $-kT\mathbf{M}(\mathbf{r}) \cdot \nabla P_0^\infty(\mathbf{r})$, to the integrand of (4.12) for the periodic or so-called "discontinuous" [12] macrotransport case, and the corresponding absence of a comparable contribution, say, $-kT\mathbf{M}(\mathbf{q}) \cdot \nabla_q P_0^\infty(\mathbf{q})$, from the integrand of (7.7) for the so-called "continuous" macrotransport case.

Future papers in this series will obviously require extensive numerical computations in order to analyze more realistic periodically micropatterned systems, such as the microlithographic arrays cited in the Introduction. Even so, the numerical methods and computational resources required for a parametric study of these devices via macrotransport analysis will clearly prove to be miniscule in comparison with those that would be required were one to attempt to solve the original microscale equations themselves in order to rigorously extract from (4.4)-(4.5) and (4.7)-(4.8) the macroscale chromatographic design parameters $\overline{\mathbf{M}}^*$ and $\overline{\mathbf{D}}^*$ needed to quantify the vector separation scheme. Irrespective of the geometric and physiochemical details of the particular separation problem to be considered in applications, the present paper unequivocally points out macrotransport theory's overwhelming advantages over otherwise attempting to solve the original microscale equations when analyzing vector chromatography through micropatterned devices.

# Bibliography


[1] C. Chou et al., Proc. Natl. Acad. Sci. U.S.A **96**, 13762 (1999).

[2] H. Chou, C. Spence, A. Scherer, and S. Quake, Proc. Natl. Acad. Sci. USA **96**, 11 (1999).

[3] C. Chou et al., Electrophoresis **21**, 81 (2000).

[4] S. Turner, A. Perez, A. Lopez, and H. Craighead, J. Vac. Sci. Technol. B **16**, 3835 (1998).

[5] W. D. Volkmuth and R. H. Austin, Nature **358**, 600 (1992).

[6] J. Han and H. Craighead, Science **288**, 1026 (2000).

[7] O. Mueller et al., Electrophoresis **21**, 128 (2000).

[8] J. Rossier et al., Electrophoresis **20**, 727 (1999).

[9] T. Duke and R. Austin, Phys. Rev. Lett. **80**, 1552 (1998).

[10] M. Shortreed, H. Li, W. Huang, and E. Yeung, Anal. Chem. **72**, 2879 (2000).

[11] D. Ertas, Phys. Rev. Lett. **80**, 1548 (1998).

[12] H. Brenner and D. Edwards, *Macrotransport Processes*, Butterworth-Heinemann, Boston, 1993.

[13] J. Nitsche and H. Brenner, J. Chem. Phys. **89**, 7510 (1988).

[14] M. O'Neill, K. Ranger, and H. Brenner, Phys. Fluids **29**, 913 (1986).

[15] D. Edwards, H. Brenner, and D. Wasan, *Interfacial transport processes and rheology*, Butterworth-Heinemann, Boston, 1991.

[16] R. Bird, W. Stewart, and E. Lightfoot, *Transport Phenomena*, John Wiley and Sons, New York, 1960.

[17] M. Shapiro and H. Brenner, Chem. Eng. Comm. **55**, 19 (1987).

[18] H. Brenner, Phil. Trans. Roy. Soc. (London) Ser. A. **297**, 81 (1980).

[19] H. Brenner and P. Adler, Philos. Trans. R. Soc. London, Ser. A **307**, 149 (1982).

[20] A. Billings, *Tensor properties of materials*, Wiley-Interscience, New York, 1969.

[21] H. Brenner and L. Gaydos, J. Colloid Interface Sci. **58**, 312 (1977).

[22] G. Mavrovouniotis and H. Brenner, J. Colloid Interface Sci. **124**, 269 (1988).

[23] G. Slater, P. Mayer, and P. Grossman, Electrophoresis **16**, 75 (1995).

[24] T. Gibson and M. Sepaniak, J. Chrom. B **695**, 103 (1997).

[25] M. Doi, *Introduction to polymer physics*, Oxford, Clarendon, 1997.

[26] A. Einstein, Ann. Phys. **17**, 549 (1905).